Manuscript Details

Manuscript number	CATTOD_2018_1172_R1
Title	Insights on the photocatalytic degradation processes supported by TiO2/WO3 systems. The case of ethanol and tetracycline.
Article type	Research paper

Abstract

TiO2/WO3 composites are widely in the literature as engineered systems for photocatalytic and (photo)electrochemical applications, since the presence of WO3 can promote both visible light absorption and electron transfer phenomena of TiO2. The preparation of these system, depending on the preparation method, can also affect the surface feature with respect to TiO2, modifying adsorption and performance, as well as the reaction mechanisms. Here, TiO2/WO3 composites were prepared by precipitation of WO3 onto the TiO2 surface and characterized in terms of their structural, morphological, optical and surface properties. Raman and IR spectroscopy as well as a marked shift in the isoelectric point support the preferential surface location of WO3. Samples were photocatalytically tested towards the degradation of ethanol and of tetracycline and the adsorption and degradation behaviour were studied, suggesting, in both cases, significant variations of the reaction paths by the addition of WO3.

Keywords	Tungsten oxide, intermediates, photocatalytic oxidation, surface properties, reaction mechanism

Corresponding Author	Luca Rimoldi
Corresponding Author's Institution	University of Milan
Order of Authors	Luca Rimoldi, Alessia Giordana, Giuseppina Cerrato, Ermelinda Falletta, Daniela Meroni

Submission Files Included in this PDF

File Name [File Type]

Cover Letter.doc [Cover Letter]

Answer to reviewers.docx [Response to Reviewers]

Highlights.docx [Highlights]

Graphical abstract.docx [Graphical Abstract]

Revised manuscript.docx [Manuscript File]

Figure 1.docx [Figure]

Figure 2.docx [Figure]

Figure 3.docx [Figure]

Table 1.docx [Table]

Table 2.docx [Table]

Revised Supplementary Material.docx [e-Component]

Supplementary Material for Reviewers only.docx [Supporting File]

To view all the submission files, including those not included in the PDF, click on the manuscript title on your EVISE Homepage, then click 'Download zip file'.

UNIVERSITÀ DEGLI STUDI DI MILANO
DIPARTIMENTO DI CHIMICA

Nanomaterials and Interfaces Group

Milan, October 22, 2018

Ref: CATTOD_2018_1172

Title: *Insights on the photocatalytic degradation processes supported by TiO2/WO3 systems. The case of ethanol and tetracycline.*

Dear Mr. Editor,

please find enclosed the revised version of the abovementioned manuscript. We wish to thank the Reviewers for their profitable comments and for their interest in our work.

All the comments raised by the Reviewers were seriously considered and modifications were introduced in the manuscript accordingly. A detailed response to the Reviewers' comments is attached as a separate file.

In this respect, additional measurements were carried out, leading to two new figures in the Supplementary Material. Moreover, in compliance with one of the Reviewer's request, we moved the experimental procedures used for photocatalytic tests in the main text and we extended the description of scavenger tests, adding 9 new references.

A 'tracked changes' version of the manuscript can be found in the "Supplementary material for Reviewers only" file. We feel that, thanks also to the Reviewers' suggestions, the quality of the manuscript has been now improved and shaped in a form more suitable to the *Catalysis Today* readership.

Yours sincerely, on behalf of all the Authors,

Luca Rimoldi Daniela Meroni

Dipartimento di Chimica
Via Golgi n°19 – 20133 Milano, Italy
Tel. 0250314219 email: luca.rimoldi@unimi.it; daniela.meroni@unimi.it

Reviewer 1

This is a very well written and discussed paper. The seek for a suitable catalyst able to work using sunlight is of pratical relevance. I recommend publication after some points being addressed by the authors.

We thank the Reviewer for his/her appreciation and interest in our work. In the following, our replies to his/her useful suggestions and comments are detailed.

1. More details regarding the scavenging experiments are required.
Authors' reply: Additional details concerning photocatalytic tests performed in the presence of scavengers (e.g., adopted amount of scavengers and procedure) were introduced in the Experimental Section (new Section 2.4), along with relevant literature references [new refs. 22-28].

2. Still in line with my previous comment, at least a resume of the experimental procedure must -be given in the main body of the paper;
Authors' reply: In agreement with the Reviewer's request, the procedures adopted for the photocatalytic tests, both in gas phase and in solution, were moved from the Supplementary Material to the main text (new Section 2.3).

3. Can the authors give some details about the catalysts reusability and their characterization after use?
Authors' reply: We added FTIR characterization of the samples after photocatalytic tests, both in the gas phase and in solution (new Figures S9-S10). The reusability of the samples in both cases were discussed in the text (new sentences in Section 3.2).

4. Some comaprison between the performance of this new catalysts and the benchmarket P25 should be given. Are these new catalysts better than P25 that is widely used and is commercially available?
Authors' reply: The authors tested commercial TiO_2 samples (P25 and anatase powder by Alfa Aesar) in previous works both in the case of ethanol degradation (see ref. 20) and tetracycline degradation (see ref. 17), in the same photocatalytic set ups and experimental conditions used in the present work. In both cases the commercial powders behaved similarly, both in terms of degradation rate and of reaction intermediates, to our home-made pristine

TiO_2 sample, used as reference throughout the present study. A sentence was introduced in the manuscript to clarify this point, referencing the interested reader to the results previously reported for commercial titania powders (Section 3.2).

Reviewer 2

The manuscript is an interesting paper on new substrate TiO2/WO3 (TW) for to remove the tetracycline. The substrate synthesized showed higher adsorption of tetracycline.
The manuscript is very complex and well presentation.
It is very hard work, scientific research and practical applications by identifying the most effective solutions.
The authors are congratulation.
The introduction is focused on the subject of your paper.
In this paper are included many true experimental dates.
The experiments were reproduced to identify possible errors.
Results are summarized.

We wish to thank the Reviewer for his/her interest and appreciation of our work.

Highlights

- TiO_2/WO_3 composites were prepared by a sol-gel/precipitation multistep approach.
- Due to the synthetic route the surface features of TiO_2 were strongly modified.
- HR-TEM and Raman spectroscopy proved the formation of surface WO_3 species.
- Samples were photocatalytically tested toward ethanol and tetracycline degradation.
- Both degradation reactions and their mechanisms were affected by WO_3 acidity.

Graphical abstract

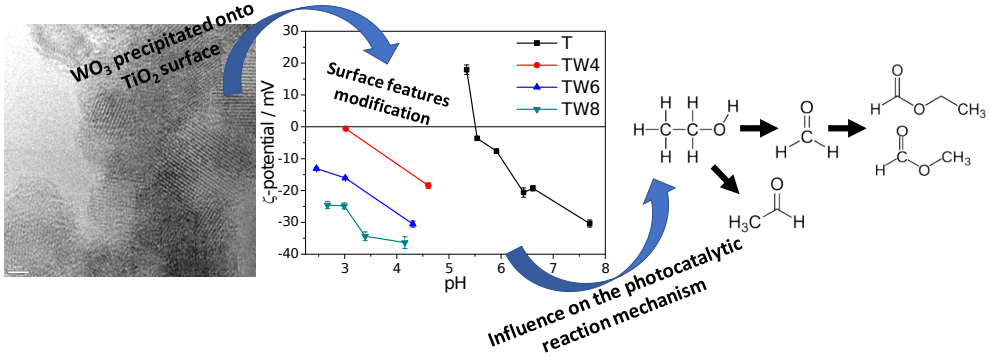

Insights on the photocatalytic degradation processes supported by TiO_2/WO_3 systems. The case of ethanol and tetracycline.

Luca Rimoldi[a,b,*], Alessia Giordana[c], Giuseppina Cerrato[c], Ermelinda Falletta[a], Daniela Meroni[a,b,*]

[a] *Dipartimento di Chimica, Università degli Studi di Milano, Via Golgi 19, 20133 Milano, Italy*

[b] *Consorzio Interuniversitario Nazionale per la Scienza e la Tecnologia dei Materiali (INSTM), Via Giusti 9, 50121 Firenze, Italy*

[c] *Dipartimento di Chimica and NIS, Inter-departmental Center, Università di Torino, Via Giuria 7, 10125 Torino, Italy*

[*]*Corresponding author: luca.rimoldi@unimi.it; daniela.meroni@unimi.it*

Abstract

TiO_2/WO_3 composites are widely in the literature as engineered systems for photocatalytic and (photo)electrochemical applications, since the presence of WO_3 can promote both visible light absorption and electron transfer phenomena of TiO_2. The preparation of these system, depending on the preparation method, can also affect the surface feature with respect to TiO_2, modifying adsorption and performance, as well as the reaction mechanisms. Here, TiO_2/WO_3 composites were prepared by precipitation of WO_3 onto the TiO_2 surface and characterized in terms of their structural, morphological, optical and surface properties. Raman and IR spectroscopy as well as a marked shift in the isoelectric point support the preferential surface location of WO_3. Samples were photocatalytically tested towards the degradation of ethanol and of tetracycline and the adsorption and degradation behaviour were studied, suggesting, in both cases, significant variations of the reaction paths by the addition of WO_3.

Keywords

Tungsten oxide, intermediates, photocatalytic oxidation, surface properties, reaction mechanism

1. Introduction

Titanium dioxide (TiO_2), due to its abundance, low-cost and stability is the most adopted semiconductor in the field of photocatalysis. However, the high e^-/h^+ recombination rate together with the large band gap (≥3.0 eV) significantly decrease the performance of TiO_2, especially under solar or visible irradiation. In order to increase the performance of TiO_2, one of the most common techniques is semiconductor engineering. In this sense, semiconductors coupling is commonly adopted for decreasing the recombination rate by exploiting charge separation effects. In this context, the band gap alignment between the coupled semiconductors is pivotal for efficient charge separation. WO_3 has been proposed as a promising semiconductor which can promote longer wavelength absorption with respect to TiO_2 thanks to its lower band gap (2.8 eV) [1] and disfavour charge recombination in composite systems. In fact, the conduction band edge of WO_3 is placed at a more positive potential than the one of TiO_2 behaving, therefore, as a sink for the photogenerated electrons while the holes remain in the TiO_2 valence band.

WO_3 has been adopted in several works for creating composite materials together with TiO_2, mainly for water splitting, fuel production, (photo)electrochemical and electrochromic applications [2–6]. The use of TiO_2/WO_3 systems for the photocatalytic degradation of organic pollutants has been described by several authors with regards to both air and water pollutants [3,7–9]. Numerous synthetic procedures have been adopted to obtain TiO_2/WO_3 both by bulk mixing of the components [3,6,10] and by surface deposition [4,11–13] showing controversial effects of the coupling. Several authors report an increase in the composite photocatalytic activity with respect to both pure oxides. Other authors obtained conflicting results [11,12]. Tada et al., in the case of TiO_2/WO_3 films, show that the photocatalytic activities for both the oxidation of CH_3-CHO in the gas phase and the liquid oxidation of 2-naftol decreased significantly with the composites [14]. This effect was rationalized as due to the decrease of the electron transfer from the semiconductors to O_2. Similarly, Miyauchi et al. reported no beneficial effects introduced by the coupling of TiO_2 and WO_3 in photocatalytic oxidation processes [15].

The aim of this work is to gather new insights pertaining the role of surface properties of TiO_2/WO_3 systems on their photocatalytic behaviour, with special attention to their reaction mechanisms. A precipitation procedure over TiO_2 sol-gel powder precursors was developed to obtain a preferential surface location of the tungsten oxide. In a previous work by our group [16], the surface location of tantalum oxide, displaying increased acidity, was observed to promote the UV degradation of ethanol in the gas phase. In the case of WO_3, its surface acidity has been related to higher pollutant adsorption at the photocatalyst surface, better dispersibility in water and enhanced $^{\bullet}OH$ radical production [11,12]. The role played by the sample composition on the structural, optical and surface

features was carefully analysed. The photocatalytic performance was tested both in the liquid and the gas phase towards two pollutants which were extensively studied by us [17–20]: an emerging pollutant (tetracycline) and ethanol as a model molecule for VOCs.

2. Experimental section

2.1 Samples synthesis

All of the reagents were purchased from Sigma-Aldrich and used without any further purification. Doubly distilled water passing through a Milli-Q apparatus was used to prepare solutions and suspensions.

The TiO_2 xerogel was prepared by sol-gel according to the following procedure. 18.4 g of titanium tetraisopropoxide (TTIP) dissolved in 24 mL of 2-propanol at 25°C was hydrolysed by adding drop by drop 113 mL of an HCl aqueous solution (pH 3) while stirring at 300 rpm. The hydrolysis was completed by stirring for other 90 min. The solid was then recovered and washed with water by five centrifugation-reprecipitation cycles. The xerogel was obtained by drying the collected solid at 90°C in an oven. TiO_2/WO_3 composites were synthesized by precipitating WO_3 on the prepared TiO_2 xerogel by a modification of a previously reported procedure [21]. The selected amount of tungstic acid (H_2WO_4) was suspended in 50 mL of water and then dissolved by addition of a 25% NH_4OH aqueous solution. Complete dissolution was typically achieved by the addition of *ca.* 1.2 mL of NH_4OH solution, when the pH value was *ca.* 10. Successively, the solution was acidified by 0.5 M HCl till pH 4 was achieved. Then, 10 mL of a 0.1 M oxalic acid solution was added (pH around 2.5), followed by the addition of 1.10 g of the prepared TiO_2 xerogel. The suspension was heated at 90°C under reflux for 6 h while stirring. The sample was then dried at 80°C and finally calcined at 450°C in O_2 flux (9 NL h^{-1}) for 6 h. The samples were labelled as TWx, where x indicate the percentage Ti/W nominal ratio (4%, 6% or 8%). This concentration range was investigated on the grounds of previous reports about optimum photocatalytic activity [3,11,21].

A pure WO_3 sample was prepared by adopting the same synthetic procedure without the addition of the TiO_2 xerogel. A reference TiO_2 sample was prepared by calcining the TiO_2 xerogel as previously described, without the addition of W salts.

2.2 Materials characterization

Detailed information regarding characterization techniques is reported in the supplementary material file.

2.3 Photocatalytic tests

The photocatalytic degradation of ethanol in the gas phase was tested under both UV (Jelosil HG500 halogenide lamp, effective power density 17 mW cm^{-2}) and visible irradiation (Lot Oriel

halogen solar lamp equipped with a UV filter for cutting off wavelengths < 400 nm, effective power density 14 mW cm^{-2}). Photocatalytic tests were carried out adopting a previously described experimental setup [19], using 50 mg of sample drop casted on a Petri dish (d = 10 cm) and a starting ethanol concentration of 198 ppm. Before irradiation, samples were kept in the dark for 20 min to achieve the adsorption equilibrium. Photolysis tests in the UV gave rise to a finale CO_2 concentration of ca. 6%. Ethanol, CO_2 and the main reaction intermediates were determined by gas chromatography (Agilent 7890).

The degradation of tetracycline hydrochloride (TC) in water was tested under UV irradiation (Jelosil HG500 halogenide lamp, effective power density 30 mW cm^{-2}) on a previously reported photocatalytic set-up [17,18] at spontaneous pH (ca. 4) and O_2 bubbling adopting a 35 ppm initial pollutant concentration and 0.5 g L^{-1} photocatalyst concentration. Before irradiation, the suspension was kept in the for 30 min to achieve an adsorption equilibrium. Photolysis tests showed less than 5% mineralization in the absence of photocatalyst under irradiation. The tetracycline concentration was monitored by UV-vis spectroscopy, measuring the absorbance at 357 nm.

2.4 Radical scavenger tests

The photocatalytic oxidation mechanism of tetracycline was investigated via radical scavengers: 2-propanol was adopted as a well known $^{\bullet}OH$ radical scavenger owing to its high rate constant of reaction with the radical (1.9 x 10^9 L mol s^{-1}) [22,23], while disodium ethylenediaminetetraacetate (Na-EDTA) was selected as h^+ scavenger species on the grounds of previous studies [24–26]. Radical scavenger tests were performed with the procedure reported in Section 2.3 except for the addition of 4.4 g of 2-propanol or 0.8 g of Na-EDTA to the tetracycline solution, in order to obtain a scavenger:TC molar ratio of 1000:1 and 30:1, respectively, in agreement with previous reports [17,26]. Moreover, photocatalytic tests were also performed under N_2 flux (9 NL h^{-1}) in order to investigate the role of O_2 on the photocatalytic performance [27,28].

3. Results and discussion

3.1 Materials characterization

The morphological features of the TW samples were investigated via N_2 adsorption-desorption isotherms collected in subcritical conditions (Fig. S1). All of the TW samples, as well as the T reference, revealed type IV profiles, typical of mesoporous materials. The hysteresis loop, centred around p/p_0 = 0.5, can be classified as H2 type, according to the IUPAC classification, usually referred to the presence of bottleneck-shaped pores. The W addition lead to a progressive increase in the specific surface area and total pore volume (Tab. 1), the latter mainly related to pores > 6 nm (Fig. S2). Previous studies [12] have reported similar increases in surface areas at low W

concentrations, which were related to the formation of a thin layer of WO_x species hindering the growth and sintering of TiO_2 particles.

The XRPD patterns of the TW samples (Fig. S3) as well as the reference T sample show a good degree of crystallinity and the typical reflections of anatase and a brookite TiO_2 polymorphs. All of the samples are composed by anatase TiO_2 as the main polymorph, while brookite is present as a minor component (Tab. 1). The TW samples show a slight increase in the brookite content, although no significant trends in the phase composition were observed with respect to the W content. No reflection peaks attributable to WO_3 phases were detected in the TW samples. Nonetheless, the XRPD pattern of the reference pristine WO_3 sample, prepared by the same precipitation route from H_2WO_4 in the absence of the TiO_2 xerogel, shows the formation of WO_3 in its monoclinic crystalline habit (Fig. S3) with hexagonal WO_3 impurities. The lack of reflections characteristic of WO_3 in TW samples reveals either the presence of highly dispersed WO_x clusters or of an amorphous WO_3 layer on TiO_2, as reported by several authors [11,12].

The average crystallite dimensions were calculated by applying the Scherrer equation on the most intense (101) reflection of anatase (Tab. 1). A slight decrease of the crystallite size is appreciable for increasing W content, in agreement with BET findings.

The HRTEM inspection of the TW samples (Fig. 1) show small crystallites, in the 4-6 nm interval, exhibiting smooth contours and closed packed nature. These values compare well with the average crystallite size obtained by elaboration of the XRPD peaks. All particles exhibit a highly ordered habit, as it is quite simple to single out fringe patterns confirming the high crystallinity of the materials. The detailed inspections of the distances of the fringe patterns, and the parallel analysis of the diffraction patterns as well, indicate that the crystallites exhibit, with very high frequency, the 0.357 nm distance, corresponding to the (101) family planes of TiO_2 anatase; this is also confirmed by the diffraction patterns marked with nr. 1 in Fig. 1. The presence of WO_x species is confirmed by the inspection of the portions of images (marked with nr. 2 in Fig. 1), in which both direct image and diffraction indicate the 0.259 nm distance, corresponding to the (131) family planes of WO_3 tungstite (ICDD card n. 00-018-1418 tungstite).

The presence of WO_3 species is also confirmed by the EDS analyses carried out for all the samples in many different portions of the grids (see a representative example in Fig. S4). The resulting W/Ti atomic ratios (Tab. 1) appear slightly lower than the stoichiometric ratios adopted in the synthetic reaction.

Micro-Raman spectra are reported in Fig. 2a. Peaks at 149, 190, 402, 517, and 638 cm^{-1} can be attributed to the 1-Eg, 2-Eg, B1g, A1g and 3-Eg modes typical of the anatase tetragonal structure [3,29], in agreement with XRPD results. All spectral components suffer of a slight shift, which can

be related to the presence of brookite [30]. Moreover, an additional peak located at ca. 970 cm^{-1} is appreciable in TW samples. This band is ascribable, on the basis of both its spectral features and literature data [31], to the W=O mode of surface tungsten-containing species in which W is present with +6 oxidation state. A preferential surface location of WO_x species can be expected as it has been reported that at least 3 mol% of WO_3 is needed to cover in a complete monolayer the much lower surface area of TiO_2 P25 [11]. It should be noted the absence of peaks at ca. 810 cm^{-1} representative of the O–W–O stretching mode of three-dimensional crystalline WO_3 [3,32] and of components in the 1050-1075 cm^{-1} range indicative of WO_x species in tetrahedral coordination [12]. These observations are in good agreement with HRTEM findings [33].

The main surface nature of the WO_3 species is also corroborated by DRS spectra (Fig. S5). With respect to the reference T sample, the W addition does not significantly modify the absorption edge of the spectra nor the band gap value (Tab. 1). The main difference between the reference and the TW samples is a visible light absorption in the 400 – 500 nm range, which can be traced back to intragap states located above the TiO_2 valence band maximum due to N-doping [34,35]. As the intensity of this spectral absorption is irrespective of the sample W content, this absorption feature can be attributed to the NH_4OH used during the TW synthesis and it seems instead unrelated with the W addition.

The surface features of the materials were investigated by zeta potential measurements as a function of pH in order to determine the isoelectric point (iep) of the samples (Fig. 2b). The bare TiO_2 material displays a slightly acidic iep (ca. 5.5), in accordance with the literature values for TiO_2 [36], especially when synthesized in acidic environment. The TW samples exhibited significant shifts of the iep towards more and more acidic values by increasing the W content. This effect can be traced back to the strongly acidic values of WO_3 which is reported to fall around or below pH 2 [36]. Specifically, the TW4 sample showed an iep around pH 3, while TW6 and TW8 showed negatively charged surface in the whole range of investigated pH. These results are in complete agreement with micro-Raman results supporting the prevailing surface location of WO_3 species.

The surface features of the samples were further investigated by FTIR spectroscopy (Fig. S6). Besides the broad absorption in the 450–850 cm^{-1} range attributed to Ti–O stretches and Ti–O–Ti vibrational modes [37], all spectra exhibit a broad band in the 3600−3000 cm^{-1} spectral range characteristic of OH stretching vibration of surface hydroxyl groups [38] and its spectral partner, the in plane H–O–H bending mode of undissociated water molecules at ca. 1630 cm^{-1}. It should be noted that the surface hydroxylation seems promoted in the case of TW, in agreement with previous reports [3]. Interestingly, the TW samples display two distinctive features with respect to pristine TiO_2: a shoulder peak at 954 cm^{-1}, attributable to stretching vibrations of W=O [39,40], and a peak

at 1438 cm^{-1}, barely visible in the case of TW4 and increasing in intensity as a function of the W content. The latter can be ascribed to NH_4^+ species, probably residues from the synthesis, coordinated to Brönsted acid sites [41,42]. This component cannot be observed in pristine TiO_2 also when NH_4OH is added during synthesis. The addition of WO_3 is known to impart Brönsted and Lewis acidity to WO_3/TiO_2 composites [11], which explains the higher surface hydroxylation [3]. It has been reported that WO_3 addition extends the desorption peak of NH_3 species toward higher temperature compared to pristine TiO_2 [12].

3.2 Photocatalytic activity

Samples were tested in the liquid phase towards the photocatalytic degradation of tetracycline under UV irradiation. Dark adsorption data are reported in Tab. 2: with the exception of TW4, an increase in TC adsorption is appreciable for TW samples with respect to the pristine TiO_2, even when normalized with respect to the specific surface area. Tetracycline is an organic molecule which presents as a mixture of its neutral and positively charged forms at spontaneous pH conditions. Hence, according to the results obtained by electrophoretic measurements, the adsorption of tetracycline on the photocatalyst surface is favoured by electrostatic effects in the case of TW samples, which are negatively charged in the adopted experimental conditions. Moreover, the presence of WO_3 induced acidic sites, clearly appreciable from FTIR results in the case of TW6 and TW8, should favour TC adsorption, as reported by the literature [3,11,43].

The reaction rates of TC disappearance together with mineralization data are reported in Tab. 2. The TW samples show slightly lower disappearance rates with respect to the reference sample and no clear trends are appreciable as a function of the W content. The most striking difference is related to the final mineralization: a clear drop of the mineralization degree is observed for increasing WO_3 amount. The photocatalyst surface at the end of TC degradation tests clearly presents adsorbed organic species, preventing the reusability of the photocatalyst, as shown by the peaks in the regions around 2900 cm^{-1} and 1700-1100 cm^{-1} in the representative ATR-FTIR spectrum reported in Fig. S7. To better understand this striking behaviour, tests with radical scavengers were carried out on both the pristine TiO_2 and the sample with the highest W content (Fig. 3a). In the case of pristine TiO_2, a main role of h^+ is apparent as shown by tests with EDTA. This is in agreement with previous reports from the literature [17,26,44]. Moreover, N_2 purging experiments showed that O_2 plays a significant role, in agreement with the literature [27,45] which has been related to a pivotal role of $O_2^{-\bullet}$ radicals in TC degradation. In the case of TW8, a more balanced effect between $^{\bullet}OH$ and h^+ species is observed, whereas O_2 species contribute to the same extent to both the T and TW8 photocatalytic reactions. Indeed, it has been previously suggested that WO_3 could be able to

generate more hydroxyl radicals thanks to its higher surface hydroxylation [11,12]. It should be noted that EDTA, besides an h^+ depletion effect, also competes for adsorption at the photocatalyst surface, as observed in the present case for both T and TW8. A different reaction mechanism can thus be hypothesized, also on the grounds of solution speciation of the reaction intermediates. UV-vis spectra show in the case of pristine TiO_2 a parallel disappearance of the absorption peaks at ca. 357 and 270 nm (Fig. S8a), which has been related to reaction mechanisms involving h^+ species [26]. Instead, the TW8 sample displays the progressive growth of the peak at 270 nm along with the disappearance of the characteristic peak of TC (Fig. S8b). The selective decrease of the peak at 357 nm is generally attributed to an initial 1,3-dipolar cycloaddition towards the C11a-C12 double-bond of a •OH radical and a consequent rearrangement with the OH at the position C12 [26,46,47]. These results are in agreement with ESI-MS spectra of TC during photocatalytic tests with TW samples upon different times of irradiation (Fig. S9), mainly showing intermediates related to •OH attack. Interestingly, a few peaks (m/z 297, 459, 475 and 477) were previously reported by us in the case of TC photocatalysis by pristine TiO_2 and attributed on the grounds of the photocatalytic mechanism reported by Zhu et al. to successive •OH attacks on the pollutant molecule [26]. In the present case, however, several more peaks can be appreciated that are generally not reported in the case of photocatalytic removal of TC by TiO_2. It is worth noting that most of them have been reported in the case of tetracyclines degradation by other advanced oxidation processes (AOPs), such as UV/H_2O_2 and catalytic ozonation [47,48]: the peaks at 413, 429, 431 m/z were attributed to the formation of TC intermediates upon alcohol oxidation mechanism, while the presence of peak 443 m/z can be traced back to the occurrence of dehydration path; the peaks at 465, 497 m/z were attributed to the influence of consecutive decarbonylation and hydroxylation paths; finally, 509 m/z peak, along with the already cited peaks at 459 and 477 m/z were attributed to progressive hydroxylations of TC. For all these degradation routes, the role of •OH is prevailing, suggesting the more important role of hydroxyl radicals for the TW composite sample, with respect to pristine TiO_2. It should be noted that the photocatalytic behaviour of the presently reported pristine TiO_2 for the degradation of tetracycline is fully comparable to that of commercial TiO_2 powders, as previously reported by us in the same experimental conditions [17].

Samples were also tested towards the degradation of ethanol in the gas phase. Dark adsorption data show an opposite trend with respect of TC: the ethanol adsorption decreases as a function of W content, more so when normalized with respect to the surface area. This observation can be rationalized considering the reported competitive adsorption at the photocatalyst surface of water and alcohols [49,50], and higher surface hydration of TiO_2-WO_3 as shown in FTIR spectra (Fig. S6). Under UV irradiation, all samples were able to completely degrade ethanol and its main

intermediate (acetaldehyde) within the reaction time (2 h). ATR-FTIR spectra of the used samples at the end of the photocatalytic tests (Figure S10) show a pristine surface, with no accumulation of carboxylic intermediates associated with photocatalyst deactivation [51–53]. At least 90% ethanol was degraded in 30 min for all samples. From the ethanol disappearance point of view, whose rate was calculated and expressed in terms of pseudo-first order kinetic constant, all samples behave similarly (Tab. 2). The variation of the rate constant among the different samples stay within the experimental error. Nonetheless, for the composite samples the production of acetaldehyde and, thus, the final conversion to CO_2 appear to be slower. In the case of TW samples, other species besides acetaldehyde, showing the typical intermediate profile, can be appreciated (Fig. 3b): they were identified by calibration with standards as formaldehyde, ethyl formate and methyl formate. Interestingly, these intermediates were never observed in our experimental setup in the case of T sample, also when a less powerful irradiation was adopted. The concentration profile of the detected reaction intermediates shows that formaldehyde forms at a similar reaction stage compared to acetaldehyde, reaching a peak concentration before 20 min of irradiation for all of the investigated samples. Formaldehyde reached its maximum concentration at similar reaction time with respect to acetaldehyde, but its degradation appears slower. Methyl formate and ethyl formate are detected later on in the reaction (up to 75 min of irradiation). It is noteworthy that WO_3 adsorbs ethanol in a dissociative mode ($CH_3CH_2O^-_{(ad)}$), due to the presence of acidic sites promoting the dissociation of H^+ from the ethanol molecule [54,55]. As previously reported by Coronado et al., with respect to molecular adsorption, the dissociative adsorption of ethanol promotes the direct formation of carboxylic acids (acetic acid and formic acid) which successively bring to oxidized species as formates [49].

The effect of the increased light absorption in the visible region leads to an enhanced visible light activity for the TW samples, especially for TW4, whose degradation kinetics almost doubled that of the reference sample (Tab. 2). In this case, a solar lamp with emission both in the UV and in the visible region but equipped with a filter able to cut off wavelengths shorter than 400 nm was adopted. As a matter of fact, the significantly lower power density with respect to the UV lamp and the limited spectral range exploited considerably decrease the ethanol degradation kinetics. The ethanol conversion was not complete within the reaction time, but in all cases acetaldehyde was produced and the ethanol degradation proceeded along the whole reaction time, thus suggesting the possibility to complete the photocatalytic oxidation reaction by prolonging the reaction time.

4. Conclusions

In the present work, TiO_2/WO_3 samples were prepared by sol-gel/precipitation multistep synthesis. Evidence from electrophoretic measurements, Raman and FTIR spectroscopies proved a preferential location of WO_3 on the surface of TiO_2. DRS spectra supported the absence of bulk effects induced by WO_3 on the optical properties of the composites. A promoted visible light absorption due to the presence of nitrogen species, imparted slightly enhanced photocatalytic activity under visible irradiation.

Thanks to the WO_3 surface acidity, TW samples showed higher adsorption of tetracycline with respect to the bare TiO_2, although lower degradation kinetics and much lower mineralization were achieved. ESI-MS analyses supported the parallel occurrence of several TC degradation pathways in the case of TW samples, in which $^{\bullet}OH$ radicals play a major role. These findings are supported also by tests with radical scavengers showing a more marked effect of $^{\bullet}OH$ radicals for TW samples with respect to TiO_2. Some of the observed reaction intermediates, not previously detected in the case of TiO_2 photocatalysis, have been reported in the case of other oxidation processes, such as catalytic ozonation and UV/H_2O_2, characterized by lower mineralization degrees. It is noteworthy that the presence of O_2 in the reaction environment plays a key role on the reaction rate for both pristine and modified TiO_2; O_2 is well known to act as electron acceptor in photocatalysis, generating $O_2^{-\bullet}$ for electron transfer by the TiO_2 conduction band ($O_2 + e^- \rightarrow O_2^{-\bullet}{}_{(aq)}$, −0.33 V NHE) and H_2O_2 for electron transfer from the WO_3 conduction band ($O_2 + 2H^+ + 2e^- \rightarrow H_2O_{2(aq)}$, +0.682 V NHE). H_2O_2 could further react with e^- to give rise to hydroxyl radicals.

Reactions in the gas phase proved how the photocatalyst surface acidity can have a detrimental role also on its adsorption features, since the competition between water and the model pollutant led to a decrease in the ethanol adsorption at the TW surface. Also in this case different reaction intermediates between TW and TiO_2 were observed. Different reaction pathways arising from the adsorption mode of the pollutant molecule were hypothesized.

Acknowledgements

Prof. Raffaella Buonsanti and Chethana Gadiyar (École Polytechnique Fédérale de Lausanne, EPFL) are gratefully acknowledged for inspiring the project and for fruitful discussion.

References

[1] C. Di Valentin, G. Pacchioni, Acc. Chem. Res. 47 (2014) 3233–3241.

[2] I.A. Castro, G. Byzynski, M. Dawson, C. Ribeiro, J. Photochem. Photobiol. A Chem. 339 (2017) 95–102.

[3] H. Khan, M.G. Rigamonti, G.S. Patience, D.C. Boffito, Appl. Catal. B Environ. 226 (2018)

311–323.
[4] N.O. Balayeva, M. Fleisch, D.W. Bahnemann, Catal. Today. 313 (2018) 63–71.
[5] J. Georgieva, E. Valova, S. Armyanov, N. Philippidis, I. Poulios, S. Sotiropoulos, J. Hazard. Mater. 211–212 (2012) 30–46.
[6] F. Riboni, M.V. Dozzi, M.C. Paganini, E. Giamello, E. Selli, Catal. Today. 287 (2017) 176–181.
[7] S.A.K. Leghari, S. Sajjad, F. Chen, J. Zhang, Chem. Eng. J. 166 (2011) 906–915.
[8] J.Y. Lee, W. Jo, J. Hazard. Mater. 314 (2016) 22–31.
[9] G. Wang, Q. Chen, Y. Liu, D. Ma, Y. Xin, X. Ma, X. Zhang, Chem. Eng. J. 337 (2018) 322–332.
[10] A. Cordero-García, G. Turnes Palomino, L. Hinojosa-Reyes, J.L. Guzmán-Mar, L. Maya-Teviño, A. Hernández-Ramírez, Environ. Sci. Pollut. Res. 24 (2017) 4613–4624.
[11] Y. Tae Kwon, K. Yong Song, W. In Lee, G. Jin Choi, Y. Rag Do, J. Catal. 191 (2000) 192–199.
[12] K.K. Akurati, A. Vital, J.-P. Dellemann, K. Michalow, T. Graule, D. Ferri, A. Baiker, Appl. Catal. B Environ. 79 (2008) 53–62.
[13] J. Han, Y. Li, L. Yang, T. Li, Y. Luo, L. Yang, S. Luo, J. Hazard. Mater. 358 (2018) 44–52.
[14] H. Tada, A. Kokubu, M. Iwasaki, S. Ito, Langmuir. 20 (2004) 4665–4670.
[15] M. Miyauchi, A. Nakajima, K. Hashimoto, T. Watanabe, Adv. Mater. 4095 (2000) 1923–1927.
[16] L. Rimoldi, D. Meroni, E. Falletta, A.M. Ferretti, A. Gervasini, G. Cappelletti, S. Ardizzone, Appl. Surf. Sci. 424 (2017) 198–205.
[17] L. Rimoldi, D. Meroni, G. Cappelletti, S. Ardizzone, Catal. Today. 281 (2017) 38–44.
[18] L. Rimoldi, E. Pargoletti, D. Meroni, E. Falletta, G. Cerrato, F. Turco, G. Cappelletti, Catal. Today. 313 (2018) 40–46.
[19] L. Rimoldi, C. Ambrosi, G. Di Liberto, L. Lo Presti, M. Ceotto, C. Oliva, D. Meroni, S. Cappelli, G. Cappelletti, G. Soliveri, S. Ardizzone, J. Phys. Chem. C. 119 (2015) 24104–24115.
[20] A. Antonello, G. Soliveri, D. Meroni, G. Cappelletti, S. Ardizzone, Catal. Today. 230 (2014) 35–40.
[21] V. Iliev, D. Tomova, S. Rakovsky, A. Eliyas, G.L. Puma, J. Mol. Catal. A Chem. 327 (2010) 51–57.
[22] Y. Chen, S. Yang, K. Wang, L. Lou, J. Photochem. Photobiol. A Chem. 172 (2005) 47–54.
[23] C. Minero, G. Mariella, V. Maurino, E. Pelizzetti, Langmuir. 16 (2000) 2632–2641.

[24] N. Serpone, I. Texier, A.V. Emeline, P. Pichat, H. Hidaka, J. Zhao, J. Photochem. Photobiol. A Chem. 136 (2000) 145–155.
[25] C. Lalhriatpuia, D. Tiwari, A. Tiwari, S.M. Lee, Chem. Eng. J. 281 (2015) 782–792.
[26] X.D. Zhu, Y.J. Wang, R.J. Sun, D.M. Zhou, Chemosphere. 92 (2013) 925–932.
[27] F. Chen, Q. Yang, J. Sun, F. Yao, S. Wang, Y. Wang, X. Wang, X. Li, C. Niu, D. Wang, G. Zeng, ACS Appl. Mater. Interfaces. 8 (2016) 32887–32900.
[28] C. Zhao, M. Pelaez, X. Duan, H. Deng, K. O'Shea, D. Fatta-Kassinos, D.D. Dionysiou, Appl. Catal. B Environ. 134–135 (2013) 83–92.
[29] H. Khan, D. Berk, Appl. Catal. A Gen. 505 (2015) 285–301.
[30] M.N. Iliev, V.G. Hadjiev, A.P. Litvinchuk, Vib. Spectrosc. 64 (2013) 148–152.
[31] M. Picquart, S. Castro-Garcia, J. Livage, C. Julien, E. Haro-Poniatowski, J. Sol-Gel Sci. Technol. 18 (2000) 199–206.
[32] W. Smith, Y. Zhao, J. Phys. Chem. C. 112 (2008) 19635–19641.
[33] M. Ahmadi, M.J.-F. Guinel, Acta Mater. 69 (2014) 203–209.
[34] D. Meroni, S. Ardizzone, G. Cappelletti, C. Oliva, M. Ceotto, D. Poelman, H. Poelman, Catal. Today. 161 (2011) 169–174.
[35] R. Asahi, T. Morikawa, H. Irie, T. Ohwaki, Chem. Rev. 114 (2014) 9824–9852.
[36] M. Kosmulski, Adv. Colloid Interface Sci. 238 (2016) 1–61.
[37] D. Guerrero-Araque, D. Ramírez-Ortega, P. Acevedo-Peña, F. Tzompantzi, H.A. Calderón, R. Gómez, J. Photochem. Photobiol. A Chem. 335 (2017) 276–286.
[38] G. Soliveri, V. Pifferi, R. Annunziata, L. Rimoldi, V. Aina, G. Cerrato, L. Falciola, G. Cappelletti, D. Meroni, J. Phys. Chem. C. 119 (2015) 15390–15400.
[39] J. Polleux, M. Antonietti, M. Niederberger, J. Mater. Chem. 16 (2006) 3969.
[40] X.-X. Zou, G.-D. Li, P.-P. Wang, J. Su, J. Zhao, L.-J. Zhou, Y.-N. Wang, J.-S. Chen, Dalt. Trans. 41 (2012) 9773.
[41] K.A. Michalow-Mauke, Y. Lu, K. Kowalski, T. Graule, M. Nachtegaal, O. Kröcher, D. Ferri, ACS Catal. 5 (2015) 5657–5672.
[42] J.J. Murcia, M.C. Hidalgo, J.A. Navío, J. Araña, J.M. Doña-Rodríguez, Appl. Catal. B Environ. 142–143 (2013) 205–213.
[43] K.K. Akurati, A. Vital, J. Dellemann, K. Michalow, T. Graule, D. Ferri, A. Baiker, Appl. Catal. B Environ. 79 (2008) 53–62.
[44] R.A. Palominos, M.A. Mondaca, A. Giraldo, G. Peñuela, M. Pérez-Moya, H.D. Mansilla, Catal. Today. 144 (2009) 100–105.
[45] C.-M. Jiang, M. Farmand, C.H. Wu, Y.-S. Liu, J. Guo, W.S. Drisdell, J.K. Cooper, I.D.

Sharp, Chem. Mater. 29 (2017) 3334–3345.
[46] Y. Wang, H. Zhang, J. Zhang, C. Lu, Q. Huang, J. Wu, F. Liu, J. Hazard. Mater. 192 (2011) 35–43.
[47] Y. Wang, H. Zhang, L. Chen, Catal. Today. 175 (2011) 283–292.
[48] Y. Liu, X. He, Y. Fu, D.D. Dionysiou, Chem. Eng. J. 284 (2016) 1317–1327.
[49] J.M. Coronado, S. Kataoka, I. Tejedor-Tejedor, M.A. Anderson, J. Catal. 219 (2003) 219–230.
[50] P. Pichat, Appl. Catal. B Environ. 99 (2010) 428–434.
[51] E. Piera, J.A. Ayllón, X. Doménech, J. Peral, Catal. Today. 76 (2002) 259–270.
[52] Z. Topalian, B.I. Stefanov, C.G. Granqvist, L. Österlund, J. Catal. 307 (2013) 265–274.
[53] F. Guzman, S.S.C. Chuang, J. Am. Chem. Soc. 132 (2010) 1502–1503.
[54] A. Labidi, C. Lambert-Mauriat, C. Jacolin, M. Bendahan, M. Maaref, K. Aguir, Sensors Actuators B Chem. 119 (2006) 374–379.
[55] W. Yu-De, C. Zhan-Xian, L. Yan-Feng, Z. Zhen-Lai, W. Xing-Hui, Solid. State. Electron. 45 (2001) 639–644.

Figures and tables captions

Figure 1 – HRTEM images and FFT patterns of TW4 (a), TW6 (b) and TW8 (c).

Figure 2 – a) Micro-Raman spectra of the TW materials; b) ζ-potential measurements of the samples as a function of pH.

Figure 3 – Tetracycline degradation rate constants in tests with radical scavengers and N_2 purging (a); concentration profiles for ethanol degradation intermediates under UV irradiation for T and TW8 samples (b).

Table 1 – Phase composition from XRPD analyses (A: anatase; B: brookite), anatase average crystallite dimensions (d_a^{101}), W/Ti atomic ratios obtained by EDS, specific surface area (SBET), total pore volume (V_{pores}) and apparent band gap (E_g) of the prepared samples.

Table 2 – Photocatalytic tests results for tetracycline (2^{nd}-4^{th} column) and ethanol (5^{th}-7^{th} column) degradation reactions: pseudo first order kinetic constants, *k*, dark adsorption, *Ads.*, and mineralization degree.

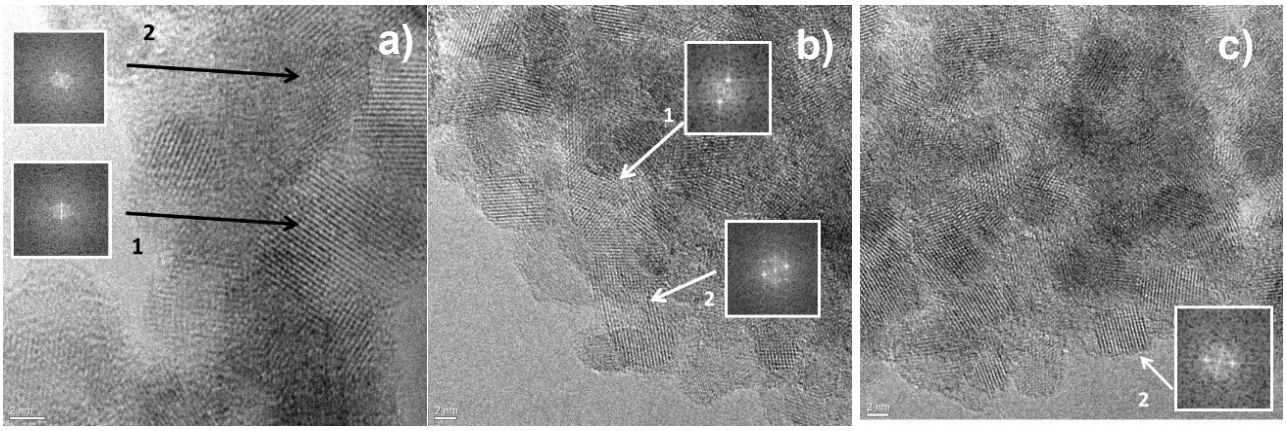

Figure 1 – HR-TEM images and FFT patterns of TW4 (a), TW6 (b) and TW8 (c).

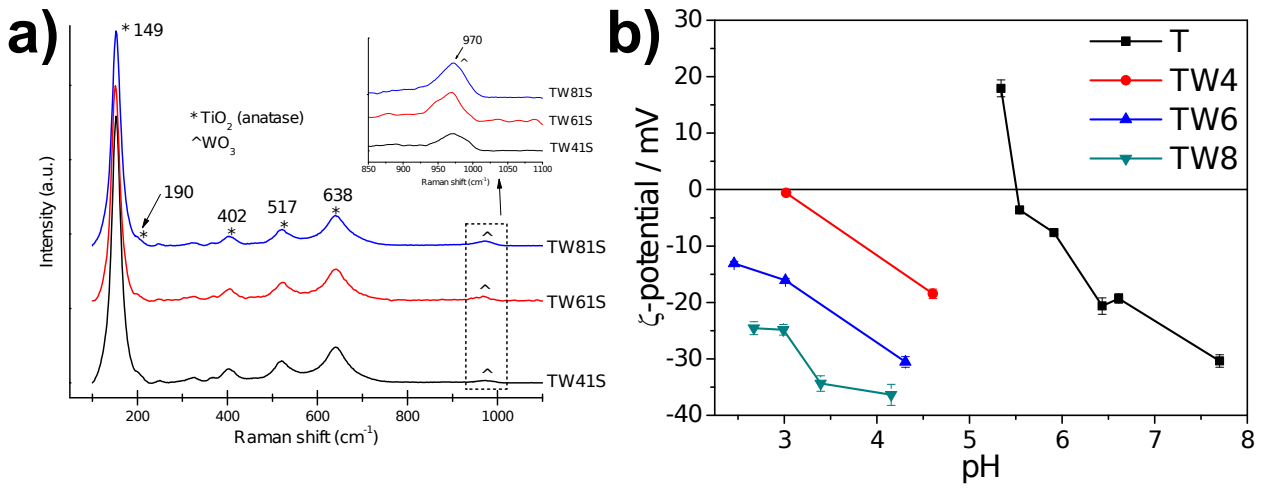

Figure 2 – a) Micro-Raman spectra of the TW materials; b) ζ-potential measurements of the samples as a function of pH

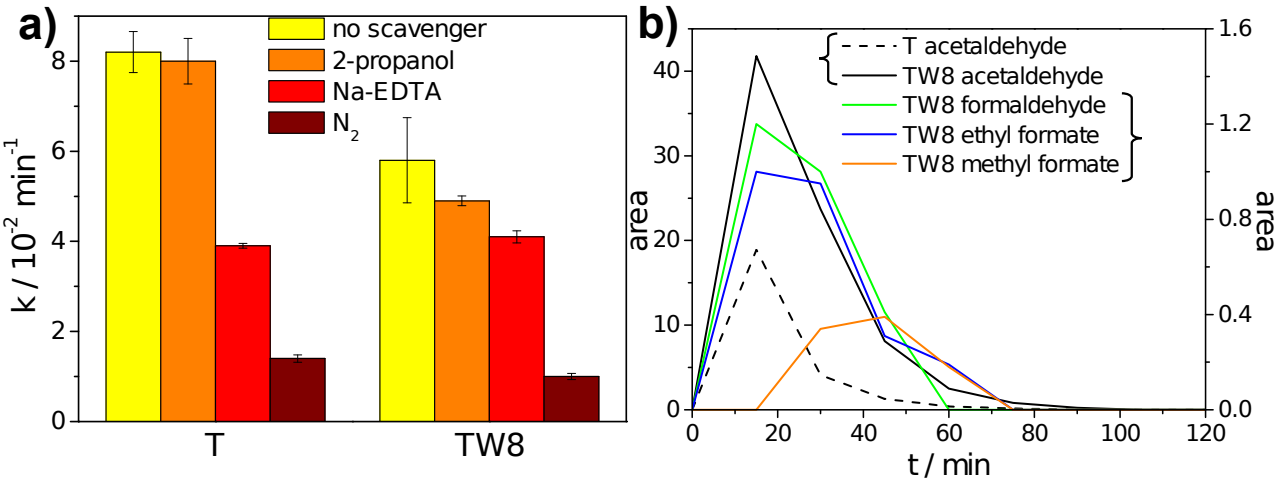

Figure 3 – Tetracycline degradation rate constants in tests with radical scavengers and N_2 purging (a); concentration profiles for ethanol degradation intermediates under UV irradiation for T and TW8 samples (b).

Sample	S_{BET} (m^2 g^{-1})	V_{pores} (mL g^{-1})	Phase composition	d_a^{101} (nm)	W/Ti at ratio (%)	E_g (eV)
T	141	0.280	75%A – 25%B	8	-	3.25
TW4	151	0.296	65%A – 35%B	7	3.1 ± 0.3	3.23
TW6	158	0.354	64%A – 36%B	6	4.8 ± 0.4	3.23
TW8	170	0.333	68%A – 32%B	6	5.3 ± 0.1	3.24

Table 1 – Phase composition from XRPD analyses (A: anatase; B: brookite), anatase average crystallite dimensions (d_a^{101}), W/Ti atomic ratios obtained by EDS, specific surface area (SBET), total pore volume (Vpores) and apparent band gap (Eg) of the prepared samples.

Sample	Tetracycline			Ethanol		
	k / min^{-1}	**Ads. / %**	**mineralization / %**	**k_{UV} / 10^{-2} min^{-1}**	**k_{vis} / 10^{-4} min^{-1}**	**Ads. / %**
T	8.2 ± 0.5	27	78	7.8 ± 0.4	3.6 ± 0.2	38
TW4	5.4 ± 0.1	23	35	7.8 ± 0.2	6.5 ± 0.1	32
TW6	6.2 ± 0.1	33	15	7.6 ± 0.2	3.4 ± 0.3	27
TW8	5.8 ± 0.9	45	7	7.7 ± 0.1	4.5 ± 0.1	26

Table 2 – Photocatalytic tests results for tetracycline (2^{nd}-4^{th} column) and ethanol (5^{th}-7^{th} column) degradation reactions: pseudo first order kinetic constants, *k*, dark adsorption, *Ads.*, and mineralization degree.

Supplementary Material

Insights on the photocatalytic degradation processes supported by TiO_2/WO_3 systems. The case of ethanol and tetracycline.

Luca Rimoldi[a,b,*], Alessia Giordana[c], Giuseppina Cerrato[c], Ermelinda Falletta[a], Chethana Gadiyar[d], Raffaella Buonsanti[d], Daniela Meroni[a,b,*]

[a] *Dipartimento di Chimica, Università degli Studi di Milano, Via Golgi 19, 20133 Milano, Italy*

[b] *Consorzio Interuniversitario Nazionale per la Scienza e la Tecnologia dei Materiali (INSTM), Via Giusti 9, 50121 Firenze, Italy*

[c] *Dipartimento di Chimica and NIS, Inter-departmental Center, Università di Torino, Via Giuria 7, 10125 Torino, Italy*

[d] *Department of Chemical Sciences and Engineering, École Polytechnique Fédérale de Lausanne, CH-1950 Sion, Switzerland*

[*] *Corresponding author: luca.rimoldi@unimi.it; daniela.meroni@unimi.it*

S1. Materials characterization

X-ray powder diffraction (XRPD) patterns were collected by adopting a Philips 3710 Bragg-Brentano goniometer. Diffractograms were collected in the 10-80° 2θ range. The Quanto software was employed to perform the Rietveld refinements and determine the phase composition of the prepared samples. The Scherrer equation was applied on the most intense peak of anatase ((101) reflection) to calculate the average crystallite dimensions.

Micro-Raman spectra were recorded on a Horiba Jobin Yvon HR800 spectrometer, equipped with a laser (532 nm) and an Olympus BX microscope.

High resolution transmission electron microscopy (HR-TEM) images of the samples were acquired with a JEOL JEM 3010 UHR operating at 300 kV, equipped with a LaB_6 filament and an Oxford Inca spectrometer for energy-dispersive X-ray spectroscopy (EDS) determinations. All powders were "dry" dispersed on Cu grids coated with lacey carbon film.

N_2 adsorption-desorption isotherms in subcritical conditions (-196°C) were measured by a Coulter 3700 instrument. The Brunauer-Emmett-Teller (BET) theory was applied to calculate the specific surface area values, while information regarding porosity were obtained by applying the Barrett-Joyner-Halenda (BJH) method.

Diffuse reflectance spectroscopy (DRS) spectra were collected in the 250-800 nm range by using a Shimadzu UV2600 UV-vis spectrophotometer.

A Malvern Zetasizer Nano instrument was adopted to determine zeta potential values from electrophoretic measurements. The samples (0.5 mg mL^{-1}) were suspended in 0.01M KNO_3. HNO_3 and KOH were used to collect zeta potential measurements as a function of pH.

Fourier transform infrared (FT-IR) spectra of the pristine and used samples were collected using a PerkinElmer Spectrum 100 FT-IR (ATR) spectrometer.

In the case of the photocatalytic degradation of tetracycline, the mineralization degree was determined by total organic carbon (TOC, Shimadzu TOC-V CPN Analyzer) measurements, while the main intermediates were studied via electrospray ionization mass spectrometry (ESI–MS) using a Thermo Finnigan LCQ Advantage MS spectrometer, equipped with an 'Ion Trap' mass analyser and an electrospray ionization source. Solutions withdrawn after different irradiation times were analyzed by direct infusion, applying a +3.0 kV potential at the capillary entrance and adopting a drying gas at 350 °C. Full-scan MS spectra were recorded in the 150–1000 m/z range.

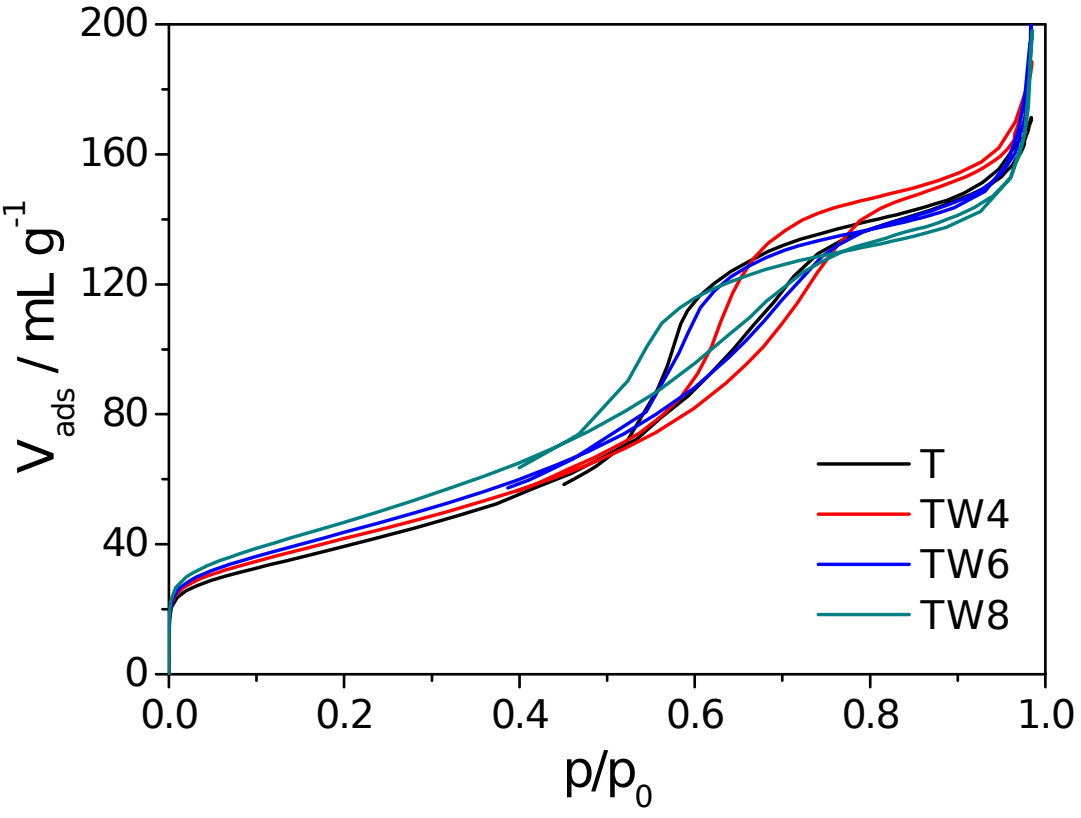

Figure S1 – N_2 adsorption-desorption isotherms at subcritical conditions (-196 °C) for TW and T samples.

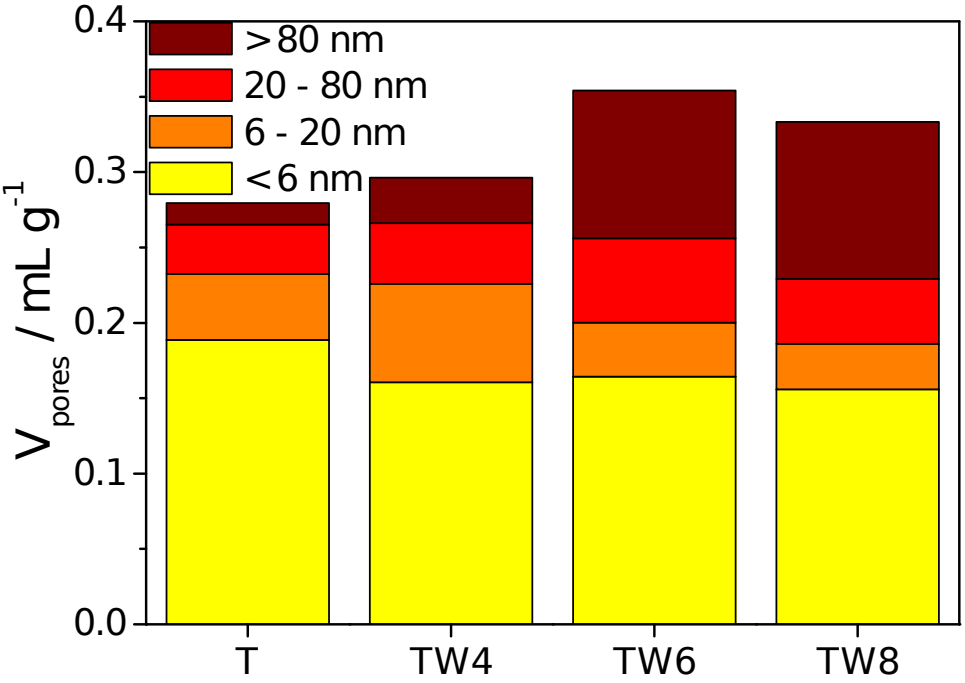

Figure S2 – Pore size distribution of T and TW samples.

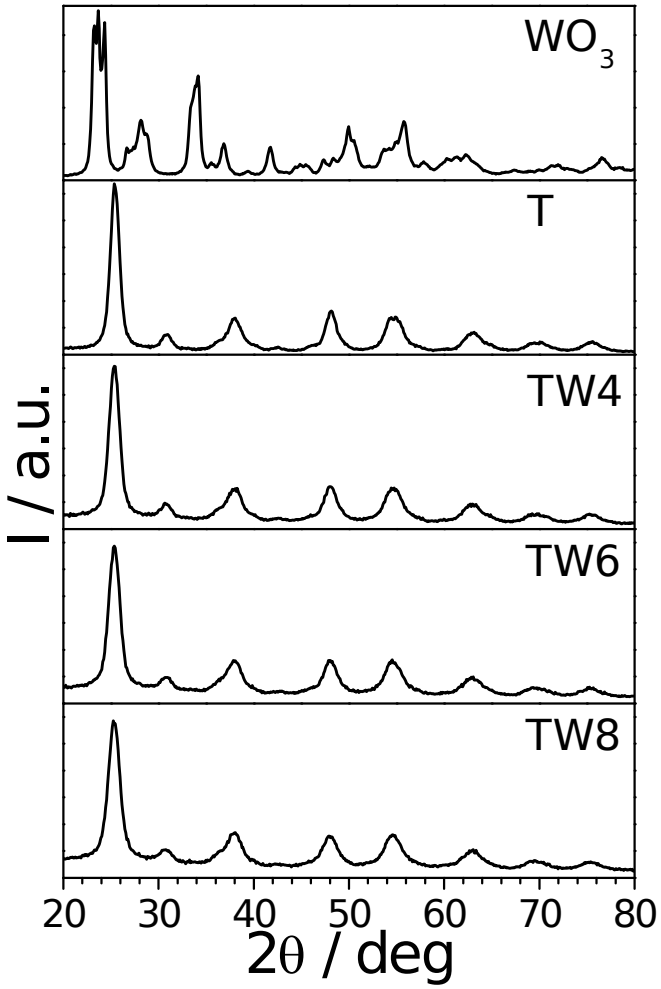

Figure S3 – XRPD patterns of the TW samples. The diffractograms of the pristine TiO_2 and WO_3 samples are added for the sake of comparison.

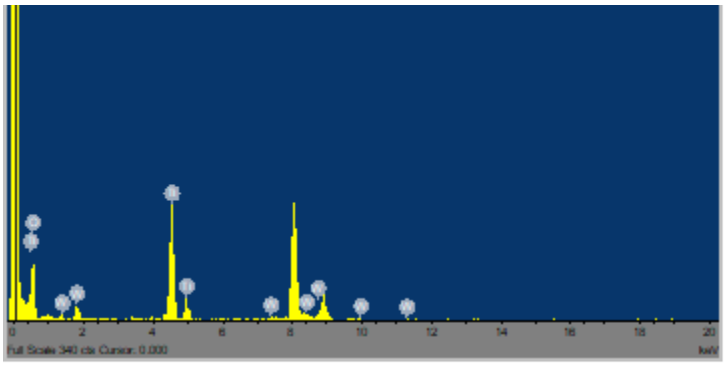

Figure S4 – EDS spectrum of the TW4 sample.

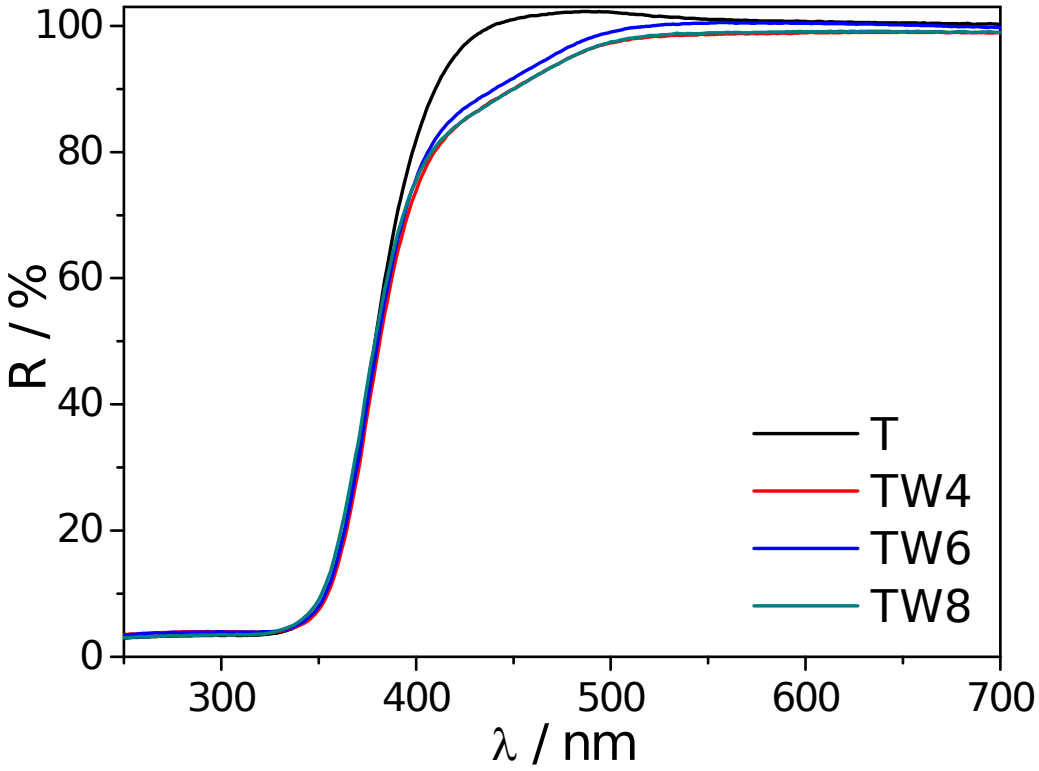

Figure S5 – DRS spectra of the TW samples. The T spectrum is also reported as reference.

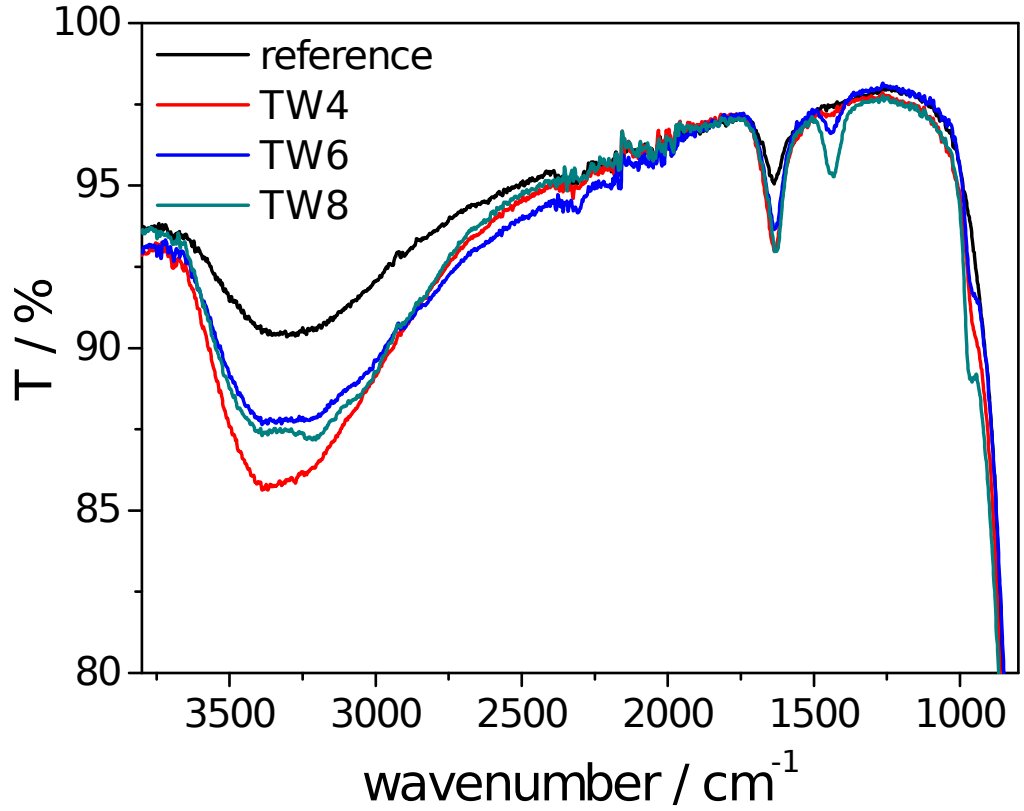

Figure S6 – FTIR spectra of the TW samples and of a reference pristine TiO_2 sample treated with NH_4OH during synthesis.

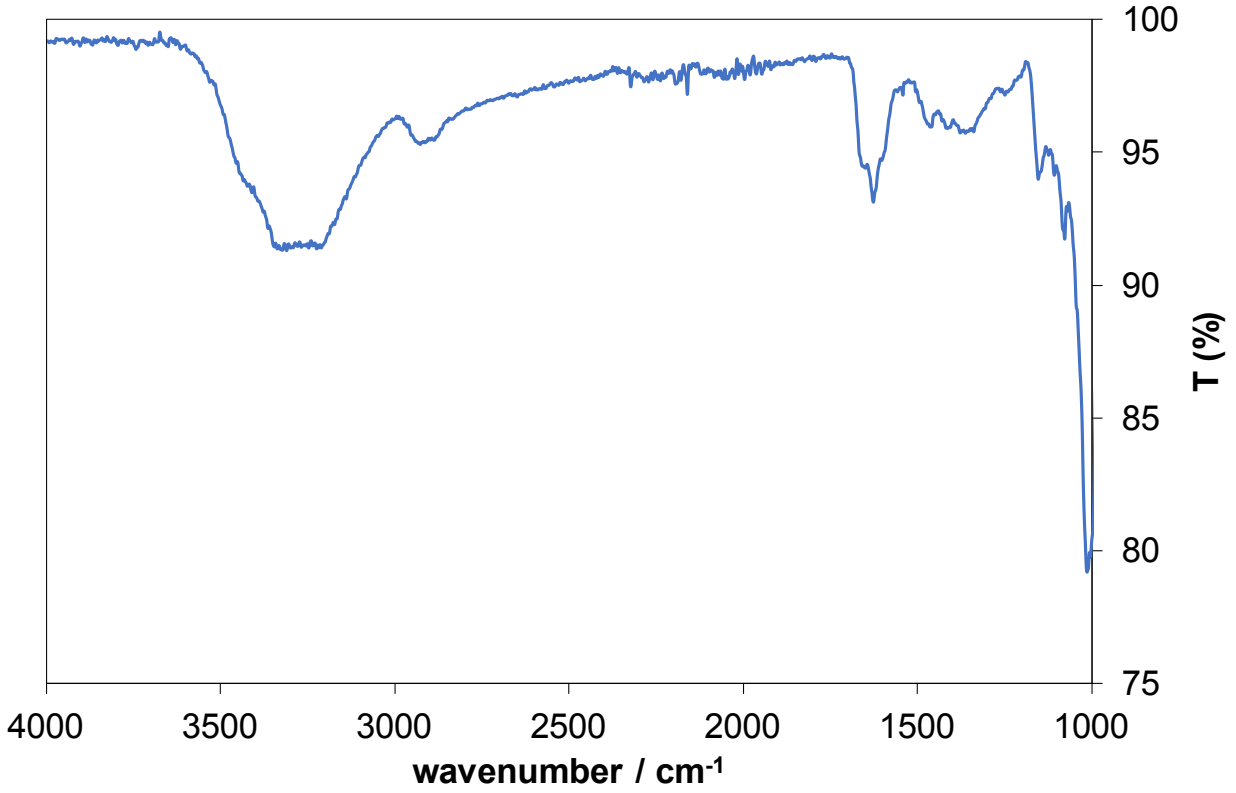

Figure S7 – FTIR spectra of TW8 after photocatalytic degradation of TC.

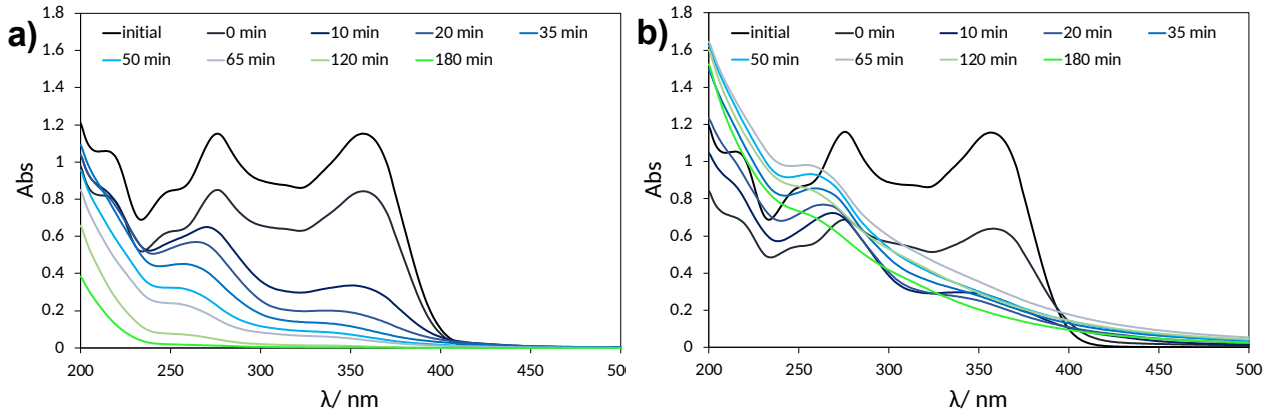

Figure S8 – UV-vis absorption spectra of TC solution with respect to time of irradiation during photocatalytic tests of T (a) and TW8 (b) photocatalysts.

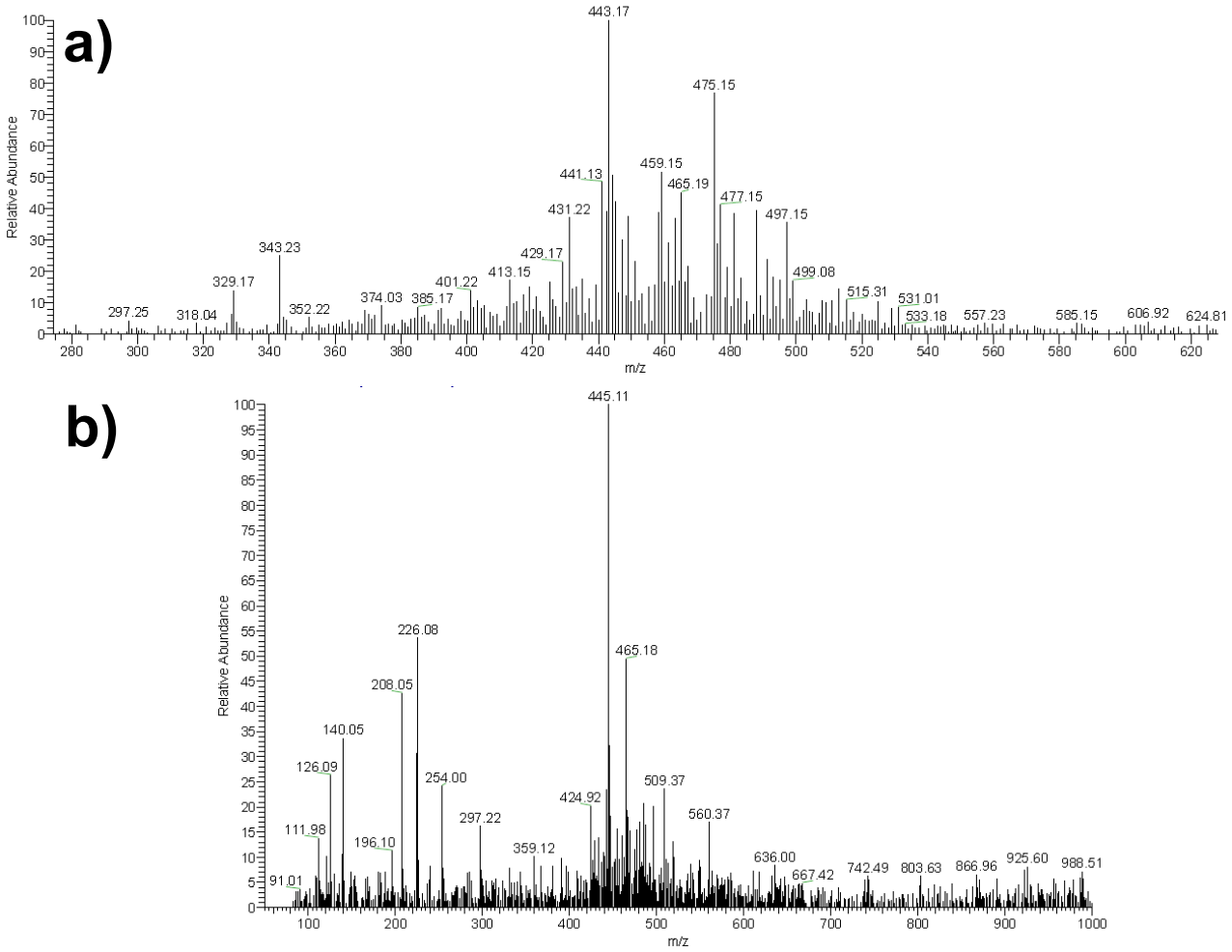

Figure S9 – ESI-MS spectra of the TW8 sample, as a representative example, after 35 min (a) and 50 min (b) UV irradiation.

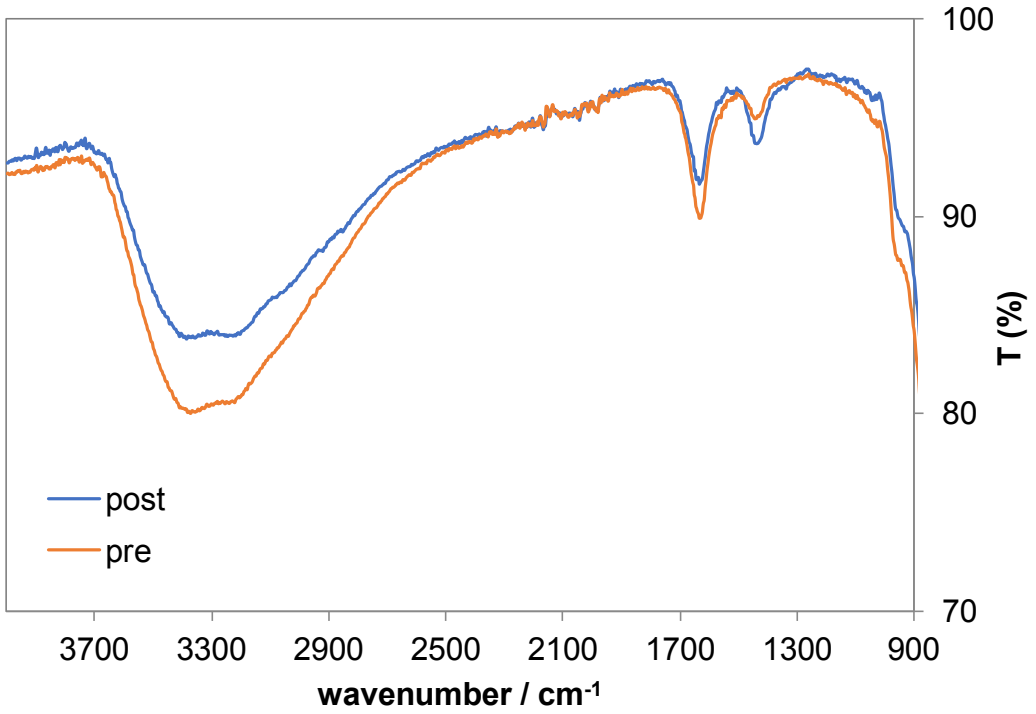

Figure S10 – FTIR spectra of TW6 sample before and after photocatalytic degradation of ethanol.

References

[1] L. Rimoldi, C. Ambrosi, G. Di Liberto, L. Lo Presti, M. Ceotto, C. Oliva, D. Meroni, S. Cappelli, G. Cappelletti, G. Soliveri, S. Ardizzone, J. Phys. Chem. C. 119 (2015) 24104–24115.

[2] L. Rimoldi, D. Meroni, G. Cappelletti, S. Ardizzone, Catal. Today. 281 (2017) 38–44.

[3] L. Rimoldi, E. Pargoletti, D. Meroni, E. Falletta, G. Cerrato, F. Turco, G. Cappelletti, Catal. Today. 313 (2018) 40–46.

Insights on the photocatalytic degradation processes supported by TiO_2/WO_3 systems. The case of ethanol and tetracycline.

Luca Rimoldi[a,b,*], Alessia Giordana[c], Giuseppina Cerrato[c], Ermelinda Falletta[a], Daniela Meroni[a,b,*]

[a] *Dipartimento di Chimica, Università degli Studi di Milano, Via Golgi 19, 20133 Milano, Italy*

[b] *Consorzio Interuniversitario Nazionale per la Scienza e la Tecnologia dei Materiali (INSTM), Via Giusti 9, 50121 Firenze, Italy*

[c] *Dipartimento di Chimica and NIS, Inter-departmental Center, Università di Torino, Via Giuria 7, 10125 Torino, Italy*

[*]*Corresponding author: luca.rimoldi@unimi.it ; daniela.meroni@unimi.it*

Abstract

TiO_2/WO_3 composites are widely in the literature as engineered systems for photocatalytic and (photo)electrochemical applications, since the presence of WO_3 can promote both visible light absorption and electron transfer phenomena of TiO_2. The preparation of these system, depending on the preparation method, can also affect the surface feature with respect to TiO_2, modifying adsorption and performance, as well as the reaction mechanisms. Here, TiO_2/WO_3 composites were prepared by precipitation of WO_3 onto the TiO_2 surface and characterized in terms of their structural, morphological, optical and surface properties. Raman and IR spectroscopy as well as a marked shift in the isoelectric point support the preferential surface location of WO_3. Samples were photocatalytically tested towards the degradation of ethanol and of tetracycline and the adsorption and degradation behaviour were studied, suggesting, in both cases, significant variations of the reaction paths by the addition of WO_3.

Keywords

Tungsten oxide, intermediates, photocatalytic oxidation, surface properties, reaction mechanism

1. Introduction

Titanium dioxide (TiO_2), due to its abundance, low-cost and stability is the most adopted semiconductor in the field of photocatalysis. However, the high e^-/h^+ recombination rate together with the large band gap (≥3.0 eV) significantly decrease the performance of TiO_2, especially under solar or visible irradiation. In order to increase the performance of TiO_2, one of the most common techniques is semiconductor engineering. In this sense, semiconductors coupling is commonly adopted for decreasing the recombination rate by exploiting charge separation effects. In this context, the band gap alignment between the coupled semiconductors is pivotal for efficient charge separation. WO_3 has been proposed as a promising semiconductor which can promote longer wavelength absorption with respect to TiO_2 thanks to its lower band gap (2.8 eV) [1] and disfavour charge recombination in composite systems. In fact, the conduction band edge of WO_3 is placed at a more positive potential than the one of TiO_2 behaving, therefore, as a sink for the photogenerated electrons while the holes remain in the TiO_2 valence band.

WO_3 has been adopted in several works for creating composite materials together with TiO_2, mainly for water splitting, fuel production, (photo)electrochemical and electrochromic applications [2–6]. The use of TiO_2/WO_3 systems for the photocatalytic degradation of organic pollutants has been described by several authors with regards to both air and water pollutants [3,7–9]. Numerous synthetic procedures have been adopted to obtain TiO_2/WO_3 both by bulk mixing of the components [3,6,10] and by surface deposition [4,11–13] showing controversial effects of the coupling. Several authors report an increase in the composite photocatalytic activity with respect to both pure oxides. Other authors obtained conflicting results [11,12]. Tada et al., in the case of TiO_2/WO_3 films, show that the photocatalytic activities for both the oxidation of CH_3-CHO in the gas phase and the liquid oxidation of 2-naftol decreased significantly with the composites [14]. This effect was rationalized as due to the decrease of the electron transfer from the semiconductors to O_2. Similarly, Miyauchi et al. reported no beneficial effects introduced by the coupling of TiO_2 and WO_3 in photocatalytic oxidation processes [15].

The aim of this work is to gather new insights pertaining the role of surface properties of TiO_2/WO_3 systems on their photocatalytic behaviour, with special attention to their reaction mechanisms. A precipitation procedure over TiO_2 sol-gel powder precursors was developed to obtain a preferential surface location of the tungsten oxide. In a previous work by our group [16], the surface location of tantalum oxide, displaying increased acidity, was observed to promote the UV degradation of ethanol in the gas phase. In the case of WO_3, its surface acidity has been related to higher pollutant adsorption at the photocatalyst surface, better dispersibility in water and enhanced $^{\bullet}OH$ radical production [11,12]. The role played by the sample composition on the structural, optical and surface

features was carefully analysed. The photocatalytic performance was tested both in the liquid and the gas phase towards two pollutants which were extensively studied by us [17–20]: an emerging pollutant (tetracycline) and ethanol as a model molecule for VOCs.

2. Experimental section

2.1 Samples synthesis

All of the reagents were purchased from Sigma-Aldrich and used without any further purification. Doubly distilled water passing through a Milli-Q apparatus was used to prepare solutions and suspensions.

The TiO_2 xerogel was prepared by sol-gel according to the following procedure. 18.4 g of titanium tetraisopropoxide (TTIP) dissolved in 24 mL of 2-propanol at 25°C was hydrolysed by adding drop by drop 113 mL of an HCl aqueous solution (pH 3) while stirring at 300 rpm. The hydrolysis was completed by stirring for other 90 min. The solid was then recovered and washed with water by five centrifugation-reprecipitation cycles. The xerogel was obtained by drying the collected solid at 90°C in an oven. TiO_2/WO_3 composites were synthesized by precipitating WO_3 on the prepared TiO_2 xerogel by a modification of a previously reported procedure [21]. The selected amount of tungstic acid (H_2WO_4) was suspended in 50 mL of water and then dissolved by addition of a 25% NH_4OH aqueous solution. Complete dissolution was typically achieved by the addition of *ca.* 1.2 mL of NH_4OH solution, when the pH value was *ca.* 10. Successively, the solution was acidified by 0.5 M HCl till pH 4 was achieved. Then, 10 mL of a 0.1 M oxalic acid solution was added (pH around 2.5), followed by the addition of 1.10 g of the prepared TiO_2 xerogel. The suspension was heated at 90°C under reflux for 6 h while stirring. The sample was then dried at 80°C and finally calcined at 450°C in O_2 flux (9 NL h^{-1}) for 6 h. The samples were labelled as TWx, where x indicate the percentage Ti/W nominal ratio (4%, 6% or 8%). This concentration range was investigated on the grounds of previous reports about optimum photocatalytic activity [3,11,21].

A pure WO_3 sample was prepared by adopting the same synthetic procedure without the addition of the TiO_2 xerogel. A reference TiO_2 sample was prepared by calcining the TiO_2 xerogel as previously described, without the addition of W salts.

2.2 Materials characterization ~~and photocatalytic tests~~

Detailed information regarding characterization techniques ~~and photocatalytic tests both in the water and gas phase~~,is reported in the supplementary material file.

2.3 Photocatalytic tests

The photocatalytic degradation of ethanol in the gas phase was tested under both UV (Jelosil HG500 halogenide lamp, effective power density 17 mW cm^{-2}) and visible irradiation (Lot Oriel

halogen solar lamp equipped with a UV filter for cutting off wavelengths < 400 nm, effective power density 14 mW cm^{-2}). Photocatalytic tests were carried out adopting a previously described experimental setup [19], using 50 mg of sample drop casted on a Petri dish (d = 10 cm) and a starting ethanol concentration of 198 ppm. Before irradiation, samples were kept in the dark for 20 min to achieve the adsorption equilibrium. Photolysis tests in the UV gave rise to a finale CO_2 concentration of ca. 6%. Ethanol, CO_2 and the main reaction intermediates were determined by gas chromatography (Agilent 7890).

The degradation of tetracycline hydrochloride (TC) in water was tested under UV irradiation (Jelosil HG500 halogenide lamp, effective power density 30 mW cm^{-2}) on a previously reported photocatalytic set-up [17,18] at spontaneous pH (ca. 4) and O_2 bubbling adopting a 35 ppm initial pollutant concentration and 0.5 g L^{-1} photocatalyst concentration. Before irradiation, the suspension was kept in the for 30 min to achieve an adsorption equilibrium. Photolysis tests showed less than 5% mineralization in the absence of photocatalyst under irradiation. The tetracycline concentration was monitored by UV-vis spectroscopy, measuring the absorbance at 357 nm.

2.4 Radical scavenger tests

The photocatalytic oxidation mechanism of tetracycline was investigated via radical scavengers: 2-propanol was adopted as a well known $^{\bullet}OH$ radical scavenger owing to its high rate constant of reaction with the radical (1.9 x 10^9 L mol s^{-1}) [22,23], while disodium ethylenediaminetetraacetate (Na-EDTA) was selected as h^+ scavenger species on the grounds of previous studies [24–26]. Radical scavenger tests were performed with the procedure reported in Section 2.3 except for the addition of 4.4 g of 2-propanol or 0.8 g of Na-EDTA to the tetracycline solution, in order to obtain a scavenger:TC molar ratio of 1000:1 and 30:1, respectively, in agreement with previous reports [17,26]. Moreover, photocatalytic tests were also performed under N_2 flux (9 NL h^{-1}) in order to investigate the role of O_2 on the photocatalytic performance [27,28].

3. Results and discussion

3.1 Materials characterization

The morphological features of the TW samples were investigated via N_2 adsorption-desorption isotherms collected in subcritical conditions (Fig. S1). All of the TW samples, as well as the T reference, revealed type IV profiles, typical of mesoporous materials. The hysteresis loop, centred around p/p_0 = 0.5, can be classified as H2 type, according to the IUPAC classification, usually referred to the presence of bottleneck-shaped pores. The W addition lead to a progressive increase in the specific surface area and total pore volume (Tab. 1), the latter mainly related to pores > 6 nm (Fig. S2). Previous studies [12] have reported similar increases in surface areas at low W

concentrations, which were related to the formation of a thin layer of WO_x species hindering the growth and sintering of TiO_2 particles.

The XRPD patterns of the TW samples (Fig. S3) as well as the reference T sample show a good degree of crystallinity and the typical reflections of anatase and a brookite TiO_2 polymorphs. All of the samples are composed by anatase TiO_2 as the main polymorph, while brookite is present as a minor component (Tab. 1). The TW samples show a slight increase in the brookite content, although no significant trends in the phase composition were observed with respect to the W content. No reflection peaks attributable to WO_3 phases were detected in the TW samples. Nonetheless, the XRPD pattern of the reference pristine WO_3 sample, prepared by the same precipitation route from H_2WO_4 in the absence of the TiO_2 xerogel, shows the formation of WO_3 in its monoclinic crystalline habit (Fig. S3) with hexagonal WO_3 impurities. The lack of reflections characteristic of WO_3 in TW samples reveals either the presence of highly dispersed WO_x clusters or of an amorphous WO_3 layer on TiO_2, as reported by several authors [11,12].

The average crystallite dimensions were calculated by applying the Scherrer equation on the most intense (101) reflection of anatase (Tab. 1). A slight decrease of the crystallite size is appreciable for increasing W content, in agreement with BET findings.

The HRTEM inspection of the TW samples (Fig. 1) show small crystallites, in the 4-6 nm interval, exhibiting smooth contours and closed packed nature. These values compare well with the average crystallite size obtained by elaboration of the XRPD peaks. All particles exhibit a highly ordered habit, as it is quite simple to single out fringe patterns confirming the high crystallinity of the materials. The detailed inspections of the distances of the fringe patterns, and the parallel analysis of the diffraction patterns as well, indicate that the crystallites exhibit, with very high frequency, the 0.357 nm distance, corresponding to the (101) family planes of TiO_2 anatase; this is also confirmed by the diffraction patterns marked with nr. 1 in Fig. 1. The presence of WO_x species is confirmed by the inspection of the portions of images (marked with nr. 2 in Fig. 1), in which both direct image and diffraction indicate the 0.259 nm distance, corresponding to the (131) family planes of WO_3 tungstite (ICDD card n. 00-018-1418 tungstite).

The presence of WO_3 species is also confirmed by the EDS analyses carried out for all the samples in many different portions of the grids (see a representative example in Fig. S4). The resulting W/Ti atomic ratios (Tab. 1) appear slightly lower than the stoichiometric ratios adopted in the synthetic reaction.

Micro-Raman spectra are reported in Fig. 2a. Peaks at 149, 190, 402, 517, and 638 cm^{-1} can be attributed to the 1-Eg, 2-Eg, B1g, A1g and 3-Eg modes typical of the anatase tetragonal structure [3,29], in agreement with XRPD results. All spectral components suffer of a slight shift, which can

be related to the presence of brookite [30]. Moreover, an additional peak located at ca. 970 cm^{-1} is appreciable in TW samples. This band is ascribable, on the basis of both its spectral features and literature data [31], to the W=O mode of surface tungsten-containing species in which W is present with +6 oxidation state. A preferential surface location of WO_x species can be expected as it has been reported that at least 3 mol% of WO_3 is needed to cover in a complete monolayer the much lower surface area of TiO_2 P25 [11]. It should be noted the absence of peaks at ca. 810 cm^{-1} representative of the O–W–O stretching mode of three-dimensional crystalline WO_3 [3,32] and of components in the 1050-1075 cm^{-1} range indicative of WO_x species in tetrahedral coordination [12]. These observations are in good agreement with HRTEM findings [33].

The main surface nature of the WO_3 species is also corroborated by DRS spectra (Fig. S5). With respect to the reference T sample, the W addition does not significantly modify the absorption edge of the spectra nor the band gap value (Tab. 1). The main difference between the reference and the TW samples is a visible light absorption in the 400 – 500 nm range, which can be traced back to intragap states located above the TiO_2 valence band maximum due to N-doping [34,35]. As the intensity of this spectral absorption is irrespective of the sample W content, this absorption feature can be attributed to the NH_4OH used during the TW synthesis and it seems instead unrelated with the W addition.

The surface features of the materials were investigated by zeta potential measurements as a function of pH in order to determine the isoelectric point (iep) of the samples (Fig. 2b). The bare TiO_2 material displays a slightly acidic iep (ca. 5.5), in accordance with the literature values for TiO_2 [36], especially when synthesized in acidic environment. The TW samples exhibited significant shifts of the iep towards more and more acidic values by increasing the W content. This effect can be traced back to the strongly acidic values of WO_3 which is reported to fall around or below pH 2 [36]. Specifically, the TW4 sample showed an iep around pH 3, while TW6 and TW8 showed negatively charged surface in the whole range of investigated pH. These results are in complete agreement with micro-Raman results supporting the prevailing surface location of WO_3 species.

The surface features of the samples were further investigated by FTIR spectroscopy (Fig. S6). Besides the broad absorption in the 450–850 cm^{-1} range attributed to Ti–O stretches and Ti–O–Ti vibrational modes [37], all spectra exhibit a broad band in the 3600−3000 cm^{-1} spectral range characteristic of OH stretching vibration of surface hydroxyl groups [38] and its spectral partner, the in plane H–O–H bending mode of undissociated water molecules at ca. 1630 cm^{-1}. It should be noted that the surface hydroxylation seems promoted in the case of TW, in agreement with previous reports [3]. Interestingly, the TW samples display two distinctive features with respect to pristine TiO_2: a shoulder peak at 954 cm^{-1}, attributable to stretching vibrations of W=O [39,40], and a peak

at 1438 cm^{-1}, barely visible in the case of TW4 and increasing in intensity as a function of the W content. The latter can be ascribed to NH_4^+ species, probably residues from the synthesis, coordinated to Brönsted acid sites [41,42]. This component cannot be observed in pristine TiO_2 also when NH_4OH is added during synthesis. The addition of WO_3 is known to impart Brönsted and Lewis acidity to WO_3/TiO_2 composites [11], which explains the higher surface hydroxylation [3]. It has been reported that WO_3 addition extends the desorption peak of NH_3 species toward higher temperature compared to pristine TiO_2 [12].

3.2 Photocatalytic activity

Samples were tested in the liquid phase towards the photocatalytic degradation of tetracycline under UV irradiation. Dark adsorption data are reported in Tab. 2: with the exception of TW4, an increase in TC adsorption is appreciable for TW samples with respect to the pristine TiO_2, even when normalized with respect to the specific surface area. Tetracycline is an organic molecule which presents as a mixture of its neutral and positively charged forms at spontaneous pH conditions. Hence, according to the results obtained by electrophoretic measurements, the adsorption of tetracycline on the photocatalyst surface is favoured by electrostatic effects in the case of TW samples, which are negatively charged in the adopted experimental conditions. Moreover, the presence of WO_3 induced acidic sites, clearly appreciable from FTIR results in the case of TW6 and TW8, should favour TC adsorption, as reported by the literature [3,11,43].

The reaction rates of TC disappearance together with mineralization data are reported in Tab. 2. The TW samples show slightly lower disappearance rates with respect to the reference sample and no clear trends are appreciable as a function of the W content. The most striking difference is related to the final mineralization: a clear drop of the mineralization degree is observed for increasing WO_3 amount. The photocatalyst surface at the end of TC degradation tests clearly presents adsorbed organic species, preventing the reusability of the photocatalyst, as shown by the peaks in the regions around 2900 cm^{-1} and 1700-1100 cm^{-1} in the representative ATR-FTIR spectrum reported in Fig. S7. To better understand this striking behaviour, tests with radical scavengers were carried out on both the pristine TiO_2 and the sample with the highest W content (Fig. 3a). In the case of pristine TiO_2, a main role of h^+ is apparent as shown by tests with EDTA. This is in agreement with previous reports from the literature [17,26,44]. Moreover, N_2 purging experiments showed that O_2 plays a significant role, in agreement with the literature [27,45] which has been related to a pivotal role of $O_2^{-\bullet}$ radicals in TC degradation. In the case of TW8, a more balanced effect between $^{\bullet}OH$ and h^+ species is observed, whereas O_2 species contribute to the same extent to both the T and TW8 photocatalytic reactions. Indeed, it has been previously suggested that WO_3 could be able to

generate more hydroxyl radicals thanks to its higher surface hydroxylation [11,12]. It should be noted that EDTA, besides an h^+ depletion effect, also competes for adsorption at the photocatalyst surface, as observed in the present case for both T and TW8. A different reaction mechanism can thus be hypothesized, also on the grounds of solution speciation of the reaction intermediates. UV-vis spectra show in the case of pristine TiO_2 a parallel disappearance of the absorption peaks at ca. 357 and 270 nm (Fig. S8a), which has been related to reaction mechanisms involving h^+ species [26]. Instead, the TW8 sample displays the progressive growth of the peak at 270 nm along with the disappearance of the characteristic peak of TC (Fig. S8b). The selective decrease of the peak at 357 nm is generally attributed to an initial 1,3-dipolar cycloaddition towards the C11a-C12 double-bond of a •OH radical and a consequent rearrangement with the OH at the position C12 [26,46,47]. These results are in agreement with ESI-MS spectra of TC during photocatalytic tests with TW samples upon different times of irradiation (Fig. S9), mainly showing intermediates related to •OH attack. Interestingly, a few peaks (m/z 297, 459, 475 and 477) were previously reported by us in the case of TC photocatalysis by pristine TiO_2 and attributed on the grounds of the photocatalytic mechanism reported by Zhu et al. to successive •OH attacks on the pollutant molecule [26]. In the present case, however, several more peaks can be appreciated that are generally not reported in the case of photocatalytic removal of TC by TiO_2. It is worth noting that most of them have been reported in the case of tetracyclines degradation by other advanced oxidation processes (AOPs), such as UV/H_2O_2 and catalytic ozonation [47,48]: the peaks at 413, 429, 431 m/z were attributed to the formation of TC intermediates upon alcohol oxidation mechanism, while the presence of peak 443 m/z can be traced back to the occurrence of dehydration path; the peaks at 465, 497 m/z were attributed to the influence of consecutive decarbonylation and hydroxylation paths; finally, 509 m/z peak, along with the already cited peaks at 459 and 477 m/z were attributed to progressive hydroxylations of TC. For all these degradation routes, the role of •OH is prevailing, suggesting the more important role of hydroxyl radicals for the TW composite sample, with respect to pristine TiO_2. It should be noted that the photocatalytic behaviour of the presently reported pristine TiO_2 for the degradation of tetracycline is fully comparable to that of commercial TiO_2 powders, as previously reported by us in the same experimental conditions [17].

Samples were also tested towards the degradation of ethanol in the gas phase. Dark adsorption data show an opposite trend with respect of TC: the ethanol adsorption decreases as a function of W content, more so when normalized with respect to the surface area. This observation can be rationalized considering the reported competitive adsorption at the photocatalyst surface of water and alcohols [49,50], and higher surface hydration of TiO_2-WO_3 as shown in FTIR spectra (Fig. S6). Under UV irradiation, all samples were able to completely degrade ethanol and its main

intermediate (acetaldehyde) within the reaction time (2 h). ATR-FTIR spectra of the used samples at the end of the photocatalytic tests (Figure S10) show a pristine surface, with no accumulation of carboxylic intermediates associated with photocatalyst deactivation [51–53]. At least 90% ethanol was degraded in 30 min for all samples. From the ethanol disappearance point of view, whose rate was calculated and expressed in terms of pseudo-first order kinetic constant, all samples behave similarly (Tab. 2). The variation of the rate constant among the different samples stay within the experimental error. Nonetheless, for the composite samples the production of acetaldehyde and, thus, the final conversion to CO_2 appear to be slower. In the case of TW samples, other species besides acetaldehyde, showing the typical intermediate profile, can be appreciated (Fig. 3b): they were identified by calibration with standards as formaldehyde, ethyl formate and methyl formate. Interestingly, these intermediates were never observed in our experimental setup in the case of T sample, also when a less powerful irradiation was adopted. The concentration profile of the detected reaction intermediates shows that formaldehyde forms at a similar reaction stage compared to acetaldehyde, reaching a peak concentration before 20 min of irradiation for all of the investigated samples. Formaldehyde reached its maximum concentration at similar reaction time with respect to acetaldehyde, but its degradation appears slower. Methyl formate and ethyl formate are detected later on in the reaction (up to 75 min of irradiation). It is noteworthy that WO_3 adsorbs ethanol in a dissociative mode ($CH_3CH_2O^-_{(ad)}$), due to the presence of acidic sites promoting the dissociation of H^+ from the ethanol molecule [54,55]. As previously reported by Coronado et al., with respect to molecular adsorption, the dissociative adsorption of ethanol promotes the direct formation of carboxylic acids (acetic acid and formic acid) which successively bring to oxidized species as formates [49].

The effect of the increased light absorption in the visible region leads to an enhanced visible light activity for the TW samples, especially for TW4, whose degradation kinetics almost doubled that of the reference sample (Tab. 2). In this case, a solar lamp with emission both in the UV and in the visible region but equipped with a filter able to cut off wavelengths shorter than 400 nm was adopted. As a matter of fact, the significantly lower power density with respect to the UV lamp and the limited spectral range exploited considerably decrease the ethanol degradation kinetics. The ethanol conversion was not complete within the reaction time, but in all cases acetaldehyde was produced and the ethanol degradation proceeded along the whole reaction time, thus suggesting the possibility to complete the photocatalytic oxidation reaction by prolonging the reaction time.

4. Conclusions

In the present work, TiO_2/WO_3 samples were prepared by sol-gel/precipitation multistep synthesis. Evidence from electrophoretic measurements, Raman and FTIR spectroscopies proved a preferential location of WO_3 on the surface of TiO_2. DRS spectra supported the absence of bulk effects induced by WO_3 on the optical properties of the composites. A promoted visible light absorption due to the presence of nitrogen species, imparted slightly enhanced photocatalytic activity under visible irradiation.

Thanks to the WO_3 surface acidity, TW samples showed higher adsorption of tetracycline with respect to the bare TiO_2, although lower degradation kinetics and much lower mineralization were achieved. ESI-MS analyses supported the parallel occurrence of several TC degradation pathways in the case of TW samples, in which $^{\bullet}OH$ radicals play a major role. These findings are supported also by tests with radical scavengers showing a more marked effect of $^{\bullet}OH$ radicals for TW samples with respect to TiO_2. Some of the observed reaction intermediates, not previously detected in the case of TiO_2 photocatalysis, have been reported in the case of other oxidation processes, such as catalytic ozonation and UV/H_2O_2, characterized by lower mineralization degrees. It is noteworthy that the presence of O_2 in the reaction environment plays a key role on the reaction rate for both pristine and modified TiO_2; O_2 is well known to act as electron acceptor in photocatalysis, generating $O_2^{-\bullet}$ for electron transfer by the TiO_2 conduction band ($O_2 + e^- \rightarrow O_2^{-\bullet}{}_{(aq)}$, −0.33 V NHE) and H_2O_2 for electron transfer from the WO_3 conduction band ($O_2 + 2H^+ + 2e^- \rightarrow H_2O_{2(aq)}$, +0.682 V NHE). H_2O_2 could further react with e^- to give rise to hydroxyl radicals.

Reactions in the gas phase proved how the photocatalyst surface acidity can have a detrimental role also on its adsorption features, since the competition between water and the model pollutant led to a decrease in the ethanol adsorption at the TW surface. Also in this case different reaction intermediates between TW and TiO_2 were observed. Different reaction pathways arising from the adsorption mode of the pollutant molecule were hypothesized.

Acknowledgements

Prof. Raffaella Buonsanti and Chethana Gadiyar (École Polytechnique Fédérale de Lausanne, EPFL) are gratefully acknowledged for inspiring the project and for fruitful discussion.

References

[1] C. Di Valentin, G. Pacchioni, Acc. Chem. Res. 47 (2014) 3233–3241.

[2] I.A. Castro, G. Byzynski, M. Dawson, C. Ribeiro, J. Photochem. Photobiol. A Chem. 339 (2017) 95–102.

[3] H. Khan, M.G. Rigamonti, G.S. Patience, D.C. Boffito, Appl. Catal. B Environ. 226 (2018)

311–323.
[4] N.O. Balayeva, M. Fleisch, D.W. Bahnemann, Catal. Today. 313 (2018) 63–71.
[5] J. Georgieva, E. Valova, S. Armyanov, N. Philippidis, I. Poulios, S. Sotiropoulos, J. Hazard. Mater. 211–212 (2012) 30–46.
[6] F. Riboni, M.V. Dozzi, M.C. Paganini, E. Giamello, E. Selli, Catal. Today. 287 (2017) 176–181.
[7] S.A.K. Leghari, S. Sajjad, F. Chen, J. Zhang, Chem. Eng. J. 166 (2011) 906–915.
[8] J.Y. Lee, W. Jo, J. Hazard. Mater. 314 (2016) 22–31.
[9] G. Wang, Q. Chen, Y. Liu, D. Ma, Y. Xin, X. Ma, X. Zhang, Chem. Eng. J. 337 (2018) 322–332.
[10] A. Cordero-García, G. Turnes Palomino, L. Hinojosa-Reyes, J.L. Guzmán-Mar, L. Maya-Teviño, A. Hernández-Ramírez, Environ. Sci. Pollut. Res. 24 (2017) 4613–4624.
[11] Y. Tae Kwon, K. Yong Song, W. In Lee, G. Jin Choi, Y. Rag Do, J. Catal. 191 (2000) 192–199.
[12] K.K. Akurati, A. Vital, J.-P. Dellemann, K. Michalow, T. Graule, D. Ferri, A. Baiker, Appl. Catal. B Environ. 79 (2008) 53–62.
[13] J. Han, Y. Li, L. Yang, T. Li, Y. Luo, L. Yang, S. Luo, J. Hazard. Mater. 358 (2018) 44–52.
[14] H. Tada, A. Kokubu, M. Iwasaki, S. Ito, Langmuir. 20 (2004) 4665–4670.
[15] M. Miyauchi, A. Nakajima, K. Hashimoto, T. Watanabe, Adv. Mater. 4095 (2000) 1923–1927.
[16] L. Rimoldi, D. Meroni, E. Falletta, A.M. Ferretti, A. Gervasini, G. Cappelletti, S. Ardizzone, Appl. Surf. Sci. 424 (2017) 198–205.
[17] L. Rimoldi, D. Meroni, G. Cappelletti, S. Ardizzone, Catal. Today. 281 (2017) 38–44.
[18] L. Rimoldi, E. Pargoletti, D. Meroni, E. Falletta, G. Cerrato, F. Turco, G. Cappelletti, Catal. Today. 313 (2018) 40–46.
[19] L. Rimoldi, C. Ambrosi, G. Di Liberto, L. Lo Presti, M. Ceotto, C. Oliva, D. Meroni, S. Cappelli, G. Cappelletti, G. Soliveri, S. Ardizzone, J. Phys. Chem. C. 119 (2015) 24104–24115.
[20] A. Antonello, G. Soliveri, D. Meroni, G. Cappelletti, S. Ardizzone, Catal. Today. 230 (2014) 35–40.
[21] V. Iliev, D. Tomova, S. Rakovsky, A. Eliyas, G.L. Puma, J. Mol. Catal. A Chem. 327 (2010) 51–57.
[22] Y. Chen, S. Yang, K. Wang, L. Lou, J. Photochem. Photobiol. A Chem. 172 (2005) 47–54.
[23] C. Minero, G. Mariella, V. Maurino, E. Pelizzetti, Langmuir. 16 (2000) 2632–2641.

[24] N. Serpone, I. Texier, A.V. Emeline, P. Pichat, H. Hidaka, J. Zhao, J. Photochem. Photobiol. A Chem. 136 (2000) 145–155.
[25] C. Lalhriatpuia, D. Tiwari, A. Tiwari, S.M. Lee, Chem. Eng. J. 281 (2015) 782–792.
[26] X.D. Zhu, Y.J. Wang, R.J. Sun, D.M. Zhou, Chemosphere. 92 (2013) 925–932.
[27] F. Chen, Q. Yang, J. Sun, F. Yao, S. Wang, Y. Wang, X. Wang, X. Li, C. Niu, D. Wang, G. Zeng, ACS Appl. Mater. Interfaces. 8 (2016) 32887–32900.
[28] C. Zhao, M. Pelaez, X. Duan, H. Deng, K. O'Shea, D. Fatta-Kassinos, D.D. Dionysiou, Appl. Catal. B Environ. 134–135 (2013) 83–92.
[29] H. Khan, D. Berk, Appl. Catal. A Gen. 505 (2015) 285–301.
[30] M.N. Iliev, V.G. Hadjiev, A.P. Litvinchuk, Vib. Spectrosc. 64 (2013) 148–152.
[31] M. Picquart, S. Castro-Garcia, J. Livage, C. Julien, E. Haro-Poniatowski, J. Sol-Gel Sci. Technol. 18 (2000) 199–206.
[32] W. Smith, Y. Zhao, J. Phys. Chem. C. 112 (2008) 19635–19641.
[33] M. Ahmadi, M.J.-F. Guinel, Acta Mater. 69 (2014) 203–209.
[34] D. Meroni, S. Ardizzone, G. Cappelletti, C. Oliva, M. Ceotto, D. Poelman, H. Poelman, Catal. Today. 161 (2011) 169–174.
[35] R. Asahi, T. Morikawa, H. Irie, T. Ohwaki, Chem. Rev. 114 (2014) 9824–9852.
[36] M. Kosmulski, Adv. Colloid Interface Sci. 238 (2016) 1–61.
[37] D. Guerrero-Araque, D. Ramírez-Ortega, P. Acevedo-Peña, F. Tzompantzi, H.A. Calderón, R. Gómez, J. Photochem. Photobiol. A Chem. 335 (2017) 276–286.
[38] G. Soliveri, V. Pifferi, R. Annunziata, L. Rimoldi, V. Aina, G. Cerrato, L. Falciola, G. Cappelletti, D. Meroni, J. Phys. Chem. C. 119 (2015) 15390–15400.
[39] J. Polleux, M. Antonietti, M. Niederberger, J. Mater. Chem. 16 (2006) 3969.
[40] X.-X. Zou, G.-D. Li, P.-P. Wang, J. Su, J. Zhao, L.-J. Zhou, Y.-N. Wang, J.-S. Chen, Dalt. Trans. 41 (2012) 9773.
[41] K.A. Michalow-Mauke, Y. Lu, K. Kowalski, T. Graule, M. Nachtegaal, O. Kröcher, D. Ferri, ACS Catal. 5 (2015) 5657–5672.
[42] J.J. Murcia, M.C. Hidalgo, J.A. Navío, J. Araña, J.M. Doña-Rodríguez, Appl. Catal. B Environ. 142–143 (2013) 205–213.
[43] K.K. Akurati, A. Vital, J. Dellemann, K. Michalow, T. Graule, D. Ferri, A. Baiker, Appl. Catal. B Environ. 79 (2008) 53–62.
[44] R.A. Palominos, M.A. Mondaca, A. Giraldo, G. Peñuela, M. Pérez-Moya, H.D. Mansilla, Catal. Today. 144 (2009) 100–105.
[45] C.-M. Jiang, M. Farmand, C.H. Wu, Y.-S. Liu, J. Guo, W.S. Drisdell, J.K. Cooper, I.D.

Sharp, Chem. Mater. 29 (2017) 3334–3345.

[46] Y. Wang, H. Zhang, J. Zhang, C. Lu, Q. Huang, J. Wu, F. Liu, J. Hazard. Mater. 192 (2011) 35–43.

[47] Y. Wang, H. Zhang, L. Chen, Catal. Today. 175 (2011) 283–292.

[48] Y. Liu, X. He, Y. Fu, D.D. Dionysiou, Chem. Eng. J. 284 (2016) 1317–1327.

[49] J.M. Coronado, S. Kataoka, I. Tejedor-Tejedor, M.A. Anderson, J. Catal. 219 (2003) 219–230.

[50] P. Pichat, Appl. Catal. B Environ. 99 (2010) 428–434.

[51] E. Piera, J.A. Ayllón, X. Doménech, J. Peral, Catal. Today. 76 (2002) 259–270.

[52] Z. Topalian, B.I. Stefanov, C.G. Granqvist, L. Österlund, J. Catal. 307 (2013) 265–274.

[53] F. Guzman, S.S.C. Chuang, J. Am. Chem. Soc. 132 (2010) 1502–1503.

[54] A. Labidi, C. Lambert-Mauriat, C. Jacolin, M. Bendahan, M. Maaref, K. Aguir, Sensors Actuators B Chem. 119 (2006) 374–379.

[55] W. Yu-De, C. Zhan-Xian, L. Yan-Feng, Z. Zhen-Lai, W. Xing-Hui, Solid. State. Electron. 45 (2001) 639–644.

Figures and tables captions

Figure 1 – HRTEM images and FFT patterns of TW4 (a), TW6 (b) and TW8 (c).

Figure 2 – a) Micro-Raman spectra of the TW materials; b) ζ-potential measurements of the samples as a function of pH.

Figure 3 – Tetracycline degradation rate constants in tests with radical scavengers and N_2 purging (a); concentration profiles for ethanol degradation intermediates under UV irradiation for T and TW8 samples (b).

Table 1 – Phase composition from XRPD analyses (A: anatase; B: brookite), anatase average crystallite dimensions (d_a^{101}), W/Ti atomic ratios obtained by EDS, specific surface area (SBET), total pore volume (V_{pores}) and apparent band gap (E_g) of the prepared samples.

Table 2 – Photocatalytic tests results for tetracycline (2^{nd}-4^{th} column) and ethanol (5^{th}-7^{th} column) degradation reactions: pseudo first order kinetic constants, *k*, dark adsorption, *Ads.*, and mineralization degree.